Progress in NMR Spectroscopy, Vol. 17, pp. 1–32, 1985
Printed in Great Britain.

0079–6565/85/$0.00+.50

INVESTIGATION OF THE SOLUTION STRUCTURES OF SHORT NUCLEIC ACID FRAGMENTS BY MEANS OF NUCLEAR OVERHAUSER ENHANCEMENT MEASUREMENTS

ANGELA M. GRONENBORN and G. MARIUS CLORE
Max Planck Institut für Biochemie, D8033 Martinsried bei München, West Germany

(*Received* 24 *June* 1984)

CONTENTS

1. INTRODUCTION

It is now 31 years since Watson and Crick[1] first proposed a double helical structure for DNA on the basis of the fibre diffraction data of Wilkins *et al.*[2] and Franklin and Gosling.[3] However, it is only recently, with the development of efficient and rapid methods of large scale oligonucleotide synthesis,[4] that it has been possible to obtain single crystal structures of a number of short oligonucleotides. These have comprised examples not only of the well known right-handed B[5–7] and A[8–11] families of DNA, but also of a novel left-handed family of DNA, known as Z DNA.[12–15] Moreover, the single crystal X-ray diffraction studies have revealed the structural details at atomic resolution of individual base-pairs along the helix heretofore unavailable from fibre diffraction studies which only yield the average structure of a DNA polymer.[16–18] Stereo pairs of B, A and Z DNA are illustrated in Figs 1 to 3 and their main structural features are summarized in Table 1.

Although X-ray diffraction provides extensive structural detail, the crystal and fibre structures of oligonucleotide crystals and DNA fibres are subject to crystal packing forces and local high ionic strengths,[19] and these may well account for much of the local structure variations observed. In this respect, it should be noted that whereas the structure of the self-complementary DNA dodecamer 5'd $(CGCGAATTCGCG)_2$* in the crystalline state does not exhibit a two-fold axis,[6] the structure of the

* Nucleic acids have three structural components: (i) a 5-membered sugar ring which is deoxyribose in DNA and ribose in RNA, (ii) heterocyclic bases (A, adenine; G, guanine; C, cytosine; T, thymine; U, uracyl) attached to the C1′ of the sugar ring in the β configuration and (iii) the 3′5′ phosphodiester linkage joining the individual nucleoside (i.e. base–sugar) units together.

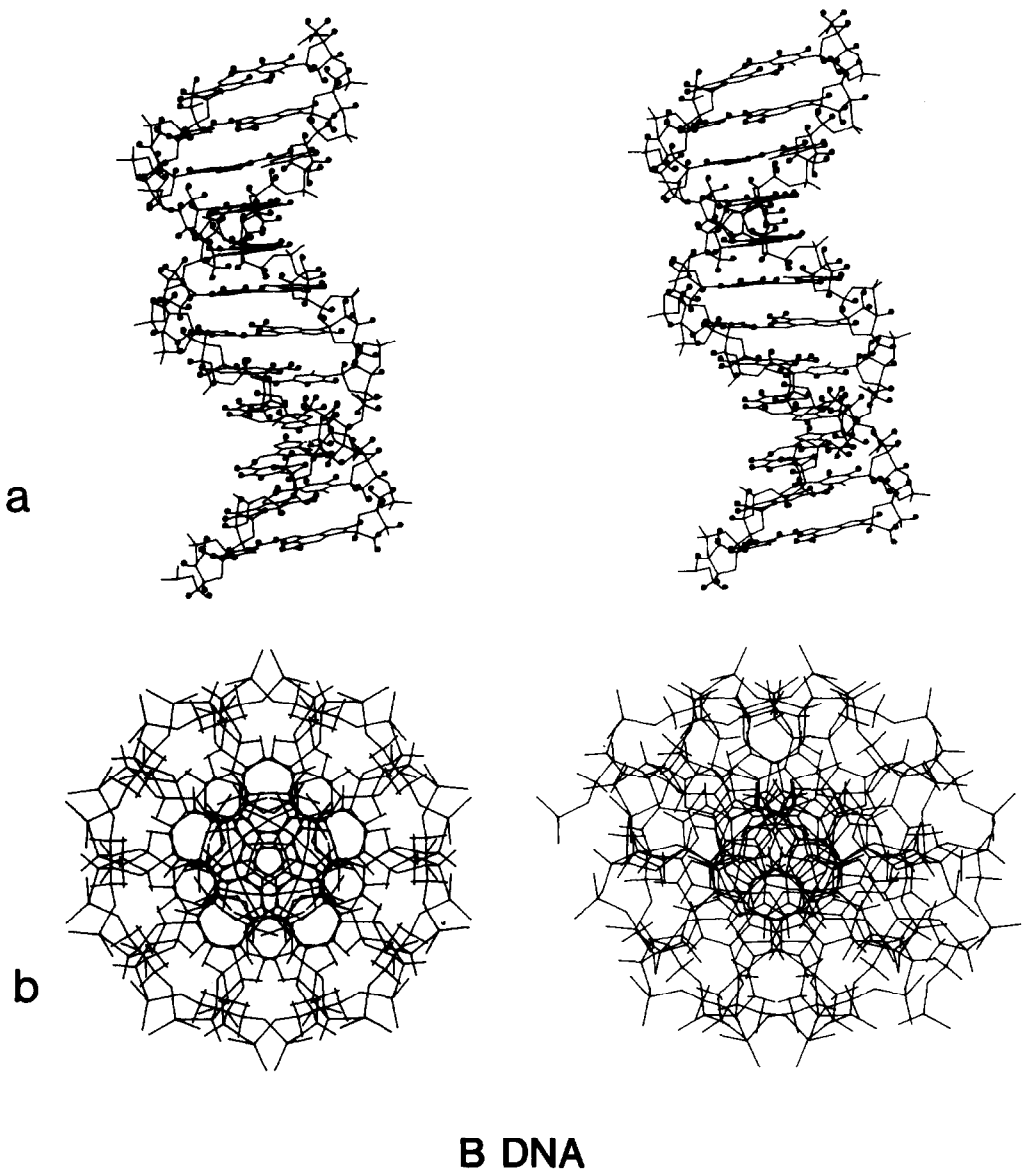

FIG. 1. Stereoview of B-DNA: (a) View parallel to the helix axis with protons highlighted, (b) view perpendicular to the helix axis.

same molecule in solution appears to be symmetric as judged by the observation of only a single set of proton resonances for each nucleotide residue.[20,21] It is therefore of considerable interest to determine the three-dimensional solution structures of oligonucleotides under physiological conditions where intermolecular interactions are less pronounced.

Short oligonucleotides are not only suitable for single crystal X-ray diffraction but also for high resolution ^{1}H-NMR studies. Consequently, their solution structures can potentially be solved, thereby enabling a comparison of the structures in the crystalline and solution states to be made. It is the purpose of this review to outline the approaches used to obtain the solution structure of such oligonucleotides.

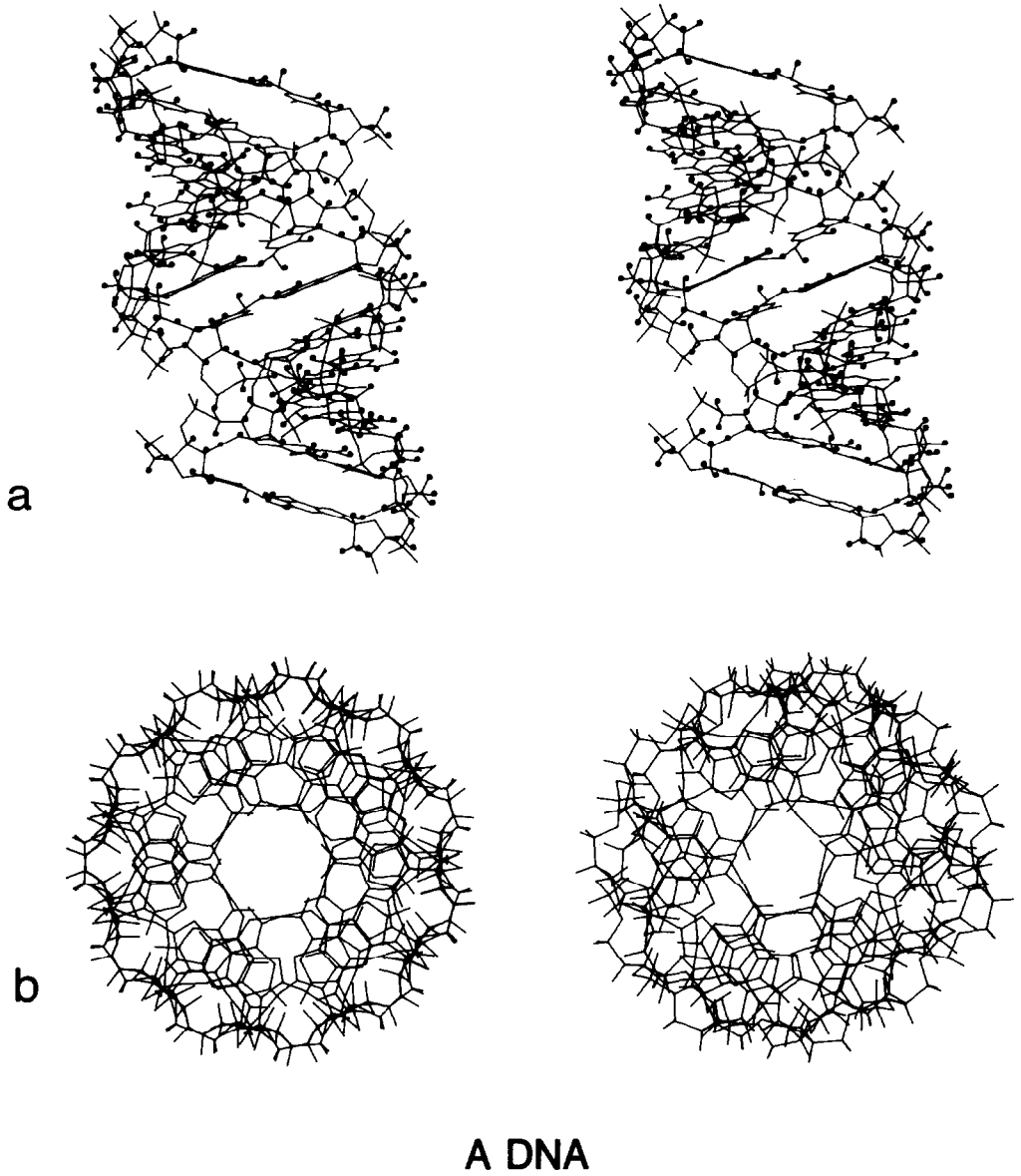

FIG. 2. Stereoview of A-DNA: (a) View parallel to the helix axis with protons highlighted, (b) view perpendicular to the helix axis.

2. NMR METHODOLOGY

2.1. *General Approaches*

Essentially there are four NMR approaches which can be used to derive structural information on an oligonucleotide in solution. The analysis of chemical shifts by the calculation of through space magnetic effects has been used but as yet is only qualitative in nature and is usually based on available crystal structure data as input parameters.[22,23] The use of paramagnetic relaxation effects is well known, but its

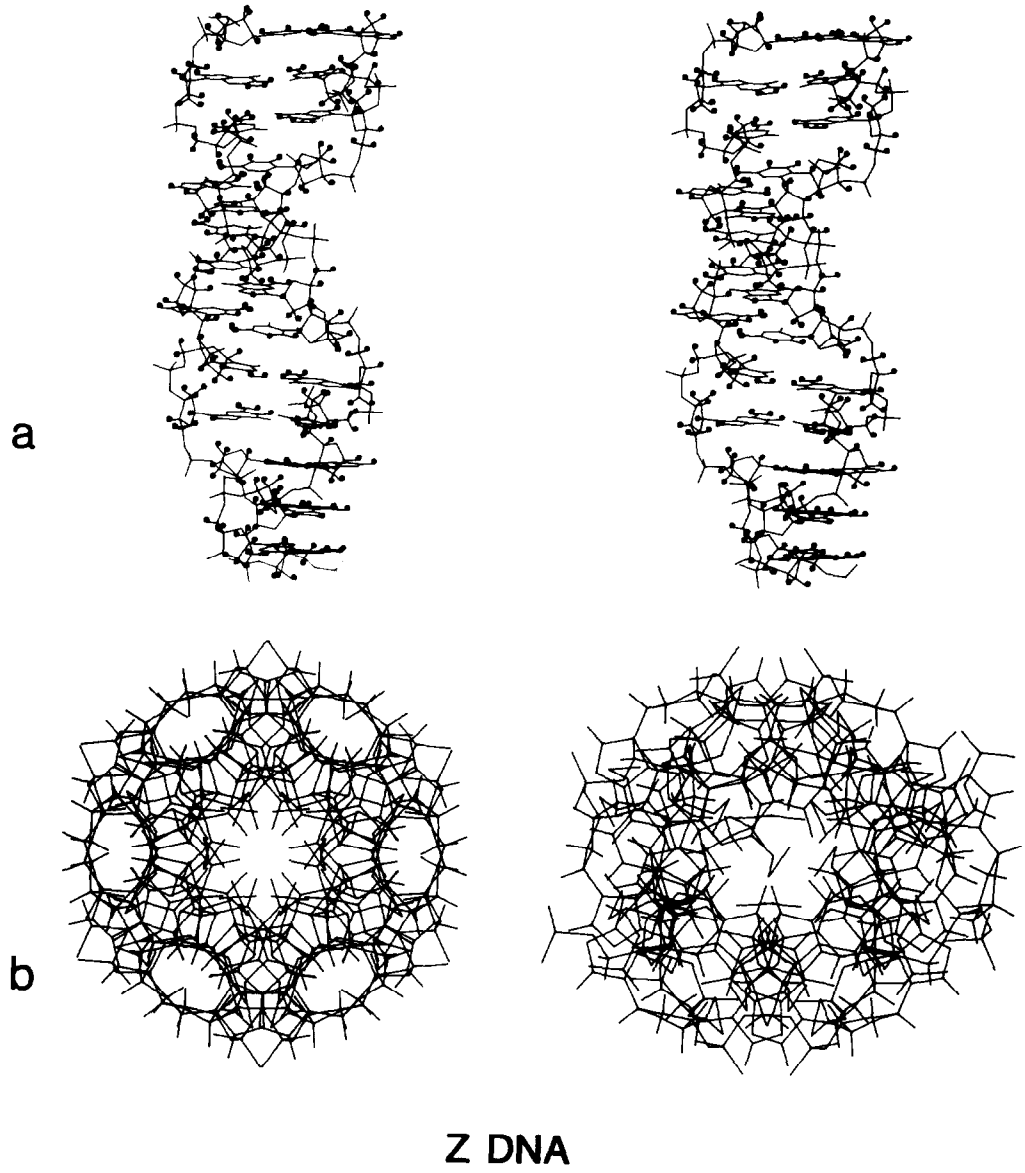

FIG. 3. Stereoview of Z-DNA: (a) View parallel to the helix axis with protons highlighted, (b) view perpendicular to the helix axis.

application is fraught with difficulties as many assumptions have to be made, particularly when an external paramagnetic probe is used.[24] The analysis of three bond spin–spin coupling constants has also been used extensively, particularly on very short oligonucleotides,[25-27] but suffers from the fact that the relation between dihedral angles and three bond spin–spin coupling constants is solely empirical in nature and the information deduced is essentially qualitative rather than quantitative.[24,28] Moreover, under conditions where oligonucleotides with six or more base-pairs are entirely double stranded, very few coupling constants are resolved sufficiently to be measured accurately, even by two-dimensional NMR techniques. Potentially the most direct and powerful method of conformational

TABLE 1. Average structural features of B, A and Z DNA (5–13)

	B	A	Z
Helix sense	right	right	left
Helix rise	~3.4 Å	~2.7 Å	~3.8 Å
Helix twist	~36°	~33°	−60°/2
Base-pairs per turn	10	11	12
Repeating unit	mononucleotide	mononucleotide	dinucleotide
Base tilt	~4°	~18°	~−8°
Ratio of groove width (major/minor)	>1	≪1	—
Ratio of groove depth (major/minor)	~1	≫1	—
Glycosidic bond conformation	anti	low anti	anti (pyrimidine) syn (purine)
Sugar pucker conformation	01′-endo to C2′-endo	C3′-endo	C2′-endo (pyrimidine) C2′-exo to C1′-exo (purine)

analysis is the use of the proton–proton nuclear Overhauser effect (NOE) to demonstrate the proximity of two protons in space and to determine their separation.[29,30] This approach has met with considerable success in the study of small proteins,[31–37] ligand–protein interactions,[38–46] nucleic acid–nucleic acid interactions,[47] transfer ribonucleic acids[48–53] and oligonucleotides.[54–67]

2.2. *The Theoretical Basis of the NOE*

The underlying basis of the NOE arises from the transfer of magnetization between two protons i and j by a process known as cross-relaxation (see Fig. 4). The cross-relaxation rate σ_{ij} between the two protons is given by the equation

$$\sigma_{ij} = \frac{\gamma^4\hbar^2}{10\langle r_{ij}^6\rangle}\left(\tau_{\text{eff}} - \frac{6\tau_{\text{eff}}}{1+4\omega^2\tau_{\text{eff}}^2}\right) \tag{1}$$

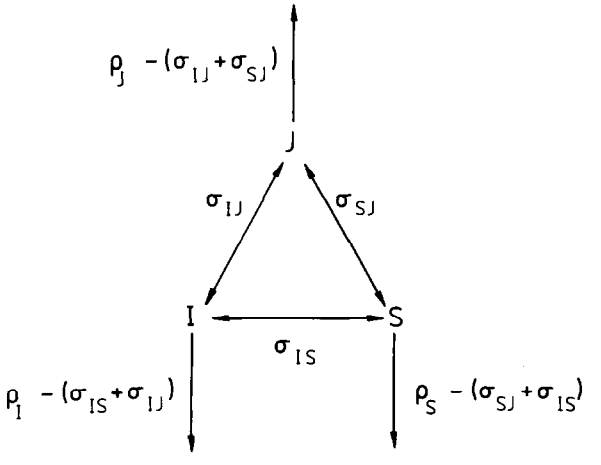

FIG. 4. Diagrammatic representation of the underlying basis of the NOE, illustrated for a three spin system. σ_{ij} and ρ_i are the cross-relaxation and total spin–lattice relaxation rates respectively. The NOE N_{ij} observed on resonance i following irradiation of resonance j for a short time t is given by $N_{ij} \sim \sigma_{ij}t$ providing $\sigma_{ij} \gtrsim \sigma_{is}$ or $\sigma_{ij} \gtrsim \sigma_{js}$.

where τ_{eff} is the effective correlation time of the i–j interproton vector, r_{ij} the distance between the two protons, ω the Larmor frequency, γ the gyromagnetic ratio of the proton, and $\hbar$ is Planck's constant divided by 2π.[68] For large molecules (MW $\gtrsim$ 1000) with long correlation times ($\tau_{eff} \gtrsim 1 \times 10^{-9}$ sec) for which $\omega\tau_{eff} > 1$, the NOEs observed are negative. However, when $\omega\tau_{eff} \gg 1$, the NOEs will no longer be selective in the steady state (i.e. following saturation of the resonance of say proton i for time $t \to \infty$ in a conventional one-dimensional experiment) owing to highly effective cross-relaxation between many protons, a phenomenon known as spin diffusion.[69] Under these conditions no structural information can be obtained. This problem can be completely circumvented by using only short times for either the selective saturation pulse in the one-dimensional experiment[70,71] or for the mixing time in the two-dimensional experiment.[72,73] In this manner, the pre-steady state NOE between two protons i and j is observed. For an irradiation time t the pre-steady state NOE, $N_{ij}(t)$, is given by

$$N_{ij}(t) \sim \sigma_{ij}t \tag{2}$$

providing $\sigma_{ij} \gtrsim \sigma_{ik}$ or $\sigma_{ij} \gtrsim \sigma_{jk}$ (where k is any other proton), as the initial build up rate of the NOE is equal to the cross-relaxation rate σ_{ij} between the two protons.[70-73] It will be noted that under these conditions the magnitude of the pre-steady state NOE observed on the resonance of any proton i is no longer dependent on the total spin lattice relaxation rate ρ_i of proton i but only on the cross-relaxation rate between protons i and j. Distance information can then be obtained as σ_{ij} is proportional to $\langle r_{ij}^{-6} \rangle$ [cf. eqn. (1)]. Thus, the ratio of two interproton distances can be obtained from the equation

$$r_{ij}/r_{k\ell} = (\sigma_{k\ell}/\sigma_{ij})^{1/6} \sim [N_{k\ell}(t)/N_{ij}(t)]^{1/6} \tag{3}$$

providing the effective correlation times of the i–j and k–ℓ interproton vectors are the same. If one of the distances is a known internal reference distance then the other interproton distance can be calculated.

Because $\sigma_{ij} \propto \langle r_{ij}^{-6} \rangle$, direct (first order) pre-steady state proton–proton NOEs are only detectable up to distances of around 5 Å, beyond which effects fall to less than -1% and become virtually undetectable. Moreover, errors introduced by the measurement of the NOE at only a single short irradiation time or mixing time, result in only small errors in interproton distance ratios, providing control experiments have been carried out to verify that the initial rate approximation given in eqn. (2) is approximately valid under these conditions. [Note that relatively small departures from the initial rate approximation have very little effect on the determination of distance ratios using eqn. (3).] Thus, a relative error of say ± 0.2 in the estimate of the ratio of two NOEs with values of -30% and -5% results in only an error of ± 0.09 in the value of the calculated distance ratio.

2.3. *Experimental Measurement of Pre-Steady State NOEs*

Considering conventional one-dimensional NMR first, the NOE experiment simply involves the saturation of the resonance of say proton i and observing the changes in intensity of the other proton resonances. In order to eliminate artefacts, this is best done using interleaved difference spectroscopy using a pulse sequence of the type

$$[(t_1\text{–}P_\alpha(\nu_i, t_2)\text{–}P_{90}\text{–AQ}(+))_m\text{–}(t_1\text{–}P_\alpha(\nu_{off}, t_2)\text{–}P_{90}\text{–AQ}(-))_m]_n \tag{4}$$

where t_1 is a relaxation delay to allow the spins to return to equilibrium between pulses, $P_\alpha(\nu_i, t_2)$ and $P_\alpha(\nu_{off}, t_2)$ are the selective on-resonance (at the position of proton i) and off-resonance saturation pulses applied for a time t_2 and AQ($\pm$) means that the signal is either added or subtracted in the computer. Typically m is 8 or 16 transients, and the cycle is then repeated n times to obtain an adequate signal-to-noise ratio.

The two-dimensional NOE experiment, known as NOESY, involves the application of a sequence of three successive non-selective 90° pulses.[73,74]

$$(90°\text{–}t_1\text{–}90°\text{–}\tau_m\text{–}90°\text{–}t_2\text{–}t_3)_n \tag{5}$$

The first 90° pulse creates transverse magnetization. During the evolution period t_1 the various magnetization components precess with their characteristic precession frequency in the x–y plane of the rotating frame and are thus frequency labelled. After the second 90° pulse, cross-relaxation leads to

incoherent magnetization exchange during the mixing time τ_m. The signal is recorded immediately after the third pulse as a function of t_2; t_3 is a fixed relaxation delay to enable the system to reach equilibrium after each recording. The experiment is repeated for a set of equidistant t_1 values. To obtain adequate signal-to-noise ratios, n transients are accumulated for each value of t_1. Two-dimensional Fourier transformation of the data matrix $s(t_1, t_2)$ then produces the desired frequency domain spectrum $s(f_1, f_2)$. Peaks corresponding to the one-dimensional spectrum appear on the diagonal, and NOE connectivities between individual lines are manifested by pairs of cross-peaks in symmetrical locations with respect to the diagonal peak.

To eliminate experimental artefacts and to suppress axial peaks and multiple quantum coherence transfer, appropriate phase cycling schemes must be used comprising typically 16 to 32 steps.[75,76] In addition, symmetrization of the NOESY spectrum is also essential to remove artefacts.[77]

Conventionally, the NOESY spectra are displayed in the absolute value mode. For small proteins of MW $\sim$ 6000 such as bovine pancreatic trypsin inhibitor, this presentation is usually adequate. In the case of oligonucleotides, however, such data handling in general leads to considerable losses in signal-to-noise. Indeed, this loss is so extensive, owing to the relatively large linewidths of many of the resonances, that the absolute value NOESY spectra of oligonucleotides are of little value. This problem can be circumvented by recording pure phase absorption NOESY spectra. This involves slightly modifying the pulse scheme given in eqn. (5). Two approaches have recently been proposed, one by States *et al.*[78] and the other by Marion and Wüthrich,[79] the latter being the simplest to implement. In essence this simply involves using the pulse scheme

$$(90°_{\Psi}-t_1-90_x-\tau_m-90_x-t_2-t_3)_n \tag{6}$$

where Ψ and x indicate the phases of the three radiofrequency pulses. Ψ is incremented at the same time as t_1 and is successively $x, y, -x, -y$. The phase incrementation amounts to an apparent change of the rotating frame frequency by half of the f_1 spectral width. As a result, a real transform of the data with respect to t_1 produces a spectrum in which positive and negative f_1 frequencies are distinguished. The benefits of the pure absorption mode NOESY spectra are highly significant in two important respects: (i) the signal-to-noise ratios are greatly improved, (ii) a true representation of cross-peak intensities is obtained.

One further technical point needs to be stated as regards the 2D NOE experiments. In addition to the transfer of magnetization by cross-relaxation during the mixing time τ_m, magnetization between J coupled spins is also transferred by multiple quantum coherence transfer. With the exception of zero quantum coherence, the latter can be eliminated by suitable phase cycling. There are several approaches that can be used to eliminate zero quantum coherence, and the simplest of these involves a random variation between 10–15 % in the value of τ_m.[74] It should also be noted that in the pure phase absorption NOESY spectra, the line shape of cross peaks arising from zero quantum coherence transfer is dispersive in both the f_1 and f_2 directions,[74] so that their total integrated intensity is zero.

The choice of 1D or 2D NOE experiments largely depends on the molecule under investigation. In very complex systems with considerable resonance overlap, there is little doubt that the 2D approach is the superior one, at least initially. However, under conditions where 1D experiments can be performed relatively easily, we tend to favour the 1D over the 2D experiment. The reason is that 1D NOE difference spectra are more reliable quantitatively than the 2D NOESY spectra. Moreover, in the 1D spectra actual NOE values are readily obtained as one can easily measure the intensity attributable to a single proton simply by measuring the intensity of the irradiated resonance (providing this is well resolved) in the NOE difference spectrum. This is essential if one wants to measure cross-relaxation rates with the purpose, for example, of obtaining the effective correlation times of fixed interproton distance vectors. In the 2D NOE experiments, however, cross-peak intensities cannot be related to the intensities of resonances along the diagonal as the latter decrease as a function of τ_m.

One further point concerning the choice of 1D and 2D experiments should be mentioned. In order to obtain a NOESY spectrum in a reasonable length of time, say less than 48 hr, the minimum concentration of material required is $\sim$3 mM. When the concentration available is less than this, it is usually preferable to perform the 1D experiment.

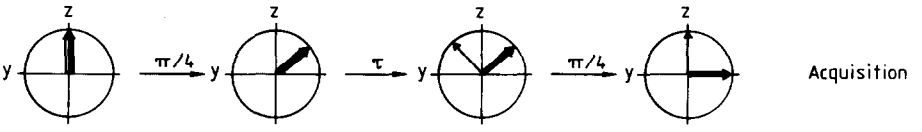

FIG. 5. Vector representation of the magnetization at the carrier frequency (thick arrow) and at $1/2\tau$ from the carrier frequency (thin arrow) in the yz plane of the rotating frame during excitation by the 1–1 pulse [eqn. (7)]. In this figure $\theta_x = \pi/4$. Prior to the first pulse all magnetization lies along the Oz axis. The first pulse flips all magnetization by an angle $\pi/4$. In the interval τ, the magnetization at the carrier frequency remains stationary whereas that at $1/2\tau$ from the carrier frequency precesses 180°. The second $\pi/4$ pulse brings the magnetization at the carrier frequency along the Oy axis and returns that $1/2\tau$ from the carrier to the Oz axis.

2.4. *Water Resonance Suppression*

In the case of oligonucleotides, the imino and amino protons undergo deuterium exchange in D_2O solution. As a result ^{1}H-NMR studies of these protons must be carried out in H_2O rather than D_2O. This necessitates the use of methods of solvent suppression in order to overcome the dynamic range and digitization problems imposed by limited word lengths of the ADC and computer. Of the methods available, the only ones appropriate to the study of the rapidly exchangeable protons found in nucleic acids are those that involve the application of excitation which has a zero spectral density at the water resonance position. This is because such methods do not involve perturbation of the exchangeable resonances by processes such as magnetization transfer, cross-relaxation or intermolecular interactions with excited water protons. Examples of the selective excitation methods include the long Alexander[80] and 2–1–4 Redfield[81] pulses and the hard time-shared Redfield,[82,83] jump-return,[84] 1–1,[85] 1–2–1[86] and higher order binomial series[87] pulses. The hard time-shared pulse sequences have the significant advantage over the long pulses that they do not require any hardware modification to existing FT spectrometers and are less sensitive to long-term drift in pulse amplitude. Of the hard pulse sequences, those that do not require phase shifting are the easiest to implement and the most effective on spectrometers not equipped with digital phase shifters. In our experience, the most effective and simplest method is the 1–1 pulse given by

$$\theta_x - \tau - \theta_x. \tag{7}$$

The carrier is placed near the region of interest, for example in the case of an oligonucleotide, in the region between the imino and aromatic proton resonances, τ is the time required for the water resonances to precess 180° in the rotating frame (namely $1/2\delta\nu$ where $\delta\nu$ is the difference in frequencies between the carrier and the resonance position of the water protons), and $2\theta_x$ is the total flip angle. After the second pulse, the magnetization of the water protons is returned to the Oz axis whilst that at the position of the carrier lies along the Oy axis. The vector representation of the magnetization behaviour in the yz plane during excitation by the 1–1 pulse sequence is shown in Fig. 5.

Figure 6 compares the 500 MHz ^{1}H-NMR spectrum of a 0.35 mM solution of the self-complementary DNA hexamer 5′d(CGTACT)$_2$ in 90% H_2O using the 1–1 (Fig. 6A), time-shared Redfield (Fig. 6B) and 1–2–1 (Fig. 6C) pulses. In all three cases the free induction decays were subjected to data shift manipulation[87,88] in order to reduce the intensity of the water peak still further thereby eliminating baseline distortions in the Fourier transformed and phase-corrected spectra. From Fig. 6 it is clear that to low field of the water peak the signal-to-noise ratios obtained using the 1–1 and time-shared Redfield pulses are comparable and slightly higher than that using the 1–2–1 pulse. To high field of the water peak, however, the signal-to-noise ratio obtained using the 1–1 pulse is much higher than that using the time-shared Redfield pulse owing to the more favourable excitation spectrum of the 1–1 pulse. It should also be noted that whereas the peaks to low and high field of the water resonance have the same phase in the case of the 1–1 and Redfield pulses, they have opposite phases in the case of the 1–2–1 pulse.

One final technical point should be mentioned. All selective excitation methods require a high degree of spectrometer stability and accuracy of both delays and pulse lengths (typically of the order of

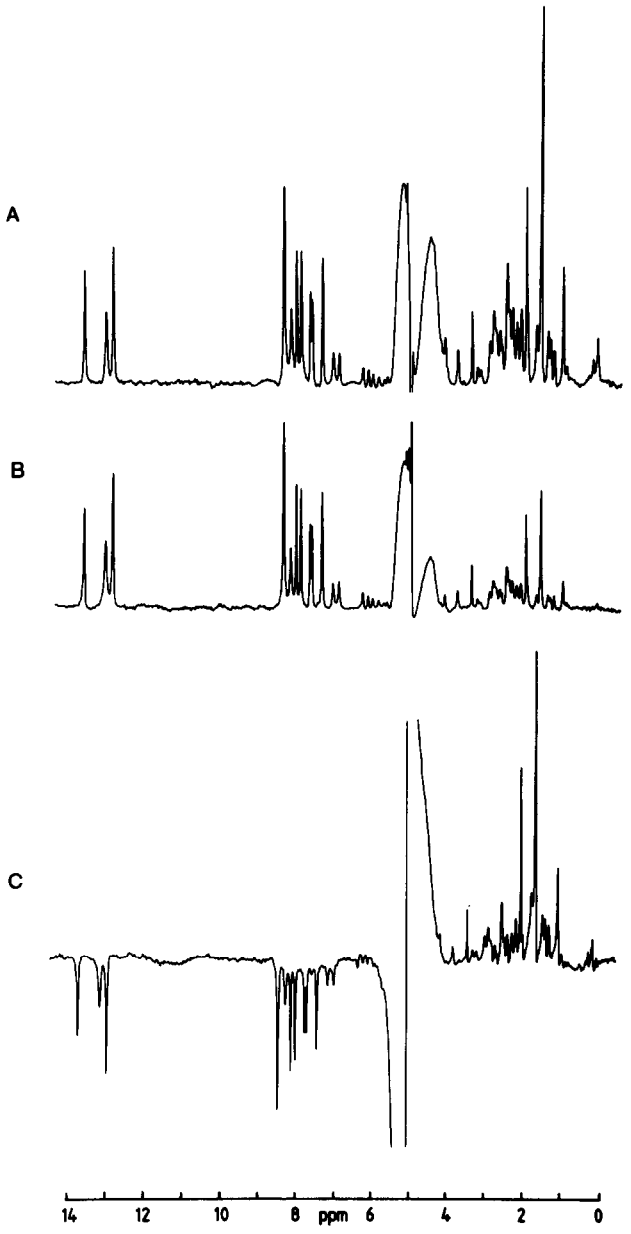

FIG. 6. 500 MHz ^{1}H-NMR spectra of a 0.35 mM solution of the DNA hexamer 5′d(CGTACG)$_2$ in 90% H_2O/10% D_2O obtained using the 1–1(A), time-share Redfield (B), and 1–2–1(C) pulses.[85] In all three cases the following instrumental conditions were used: carrier position, 3048 Hz downfield from the water resonance position; sweep width 12,195 Hz; acquisition time, 0.366 sec; interpulse delay, 0.5 sec; number of transients, 960; detection, in quadrature. In (A), (P–τ–P), P = 4.5 μsec and τ = 160.5 μsec; in (B), $(P–\tau)_{10}$, P = 0.9 μsec and τ = 31.8 μsec; in (C) (P_1–τ_1–P_2–τ_2–P_3), P_1 = 2.4 μsec, P_2 = 4.7 μsec, P_3 = 2.2 μsec, τ_1 = 163.8 μsec and τ_2 = 160.8 μsec. The time required for the water protons to precess 180° is τ in the case of the 1–1 and 1–2–1 pulses and 5τ in the case of the time-shared Redfield pulse. In all three cases prior to Fourier transformation and phase correction, the acquired FID was left shifted four times and added to the unshifted FID resulting in nulls at position 1/4W from the carrier where W is the total sweep width.[88] Experimental conditions: 0.35 mM hexamer in 90% H_2O/10% D_2O containing 1 M KCl, 50 mM potassium phosphate pH 6.5 and 0.1 mM EDTA; temperature, 5°C.

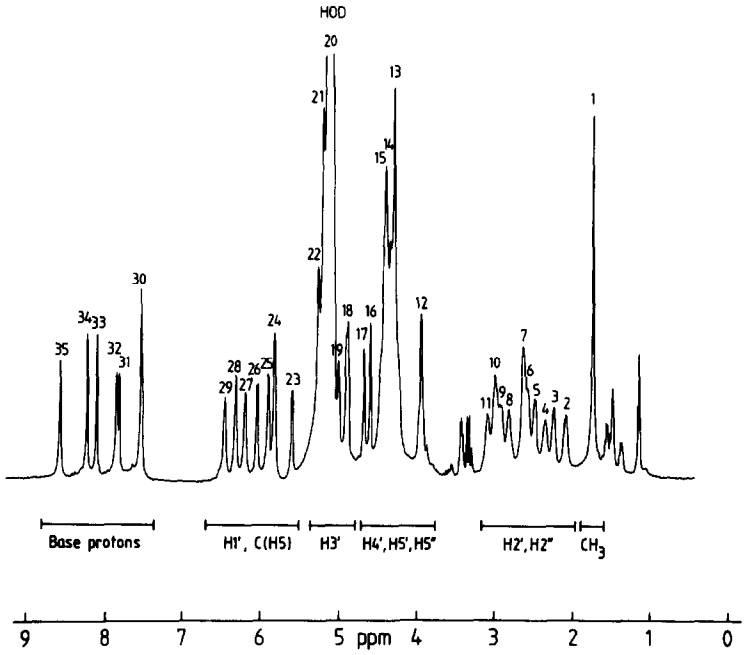

FIG. 7. 500 MHz ^{1}H-NMR spectrum between 0 and 9 ppm of the DNA hexamer 5'd(CGTACG)$_2$ in D_2O at 5°C. The non-exchangeable resonances are labelled 1–35 (see ref. 57 for assignments). Experimental conditions: 0.35 mM duplex in 99.96% D_2O containing 1 M KCl, 50 mM potassium phosphate buffer pH* 6.5 (meter reading uncorrected for the isotope effect on the glass electrode) and 0.1 mM EDTA.

0.1 μsec). Moreover, in our experience a 16-bit digitizer is essential for the successful use of these pulse sequences.

As regards the application of these selective excitation pulses to water resonance suppression in 2D NOE spectroscopy, all that is required is the replacement of the third 90° pulse in the sequences (5) and (6) by the selective excitation pulse with a total flip angle of 90°.

3. RESONANCE ASSIGNMENT

3.1. *First Level Resonance Assignment*

The assignment of resonance type is easily achieved by comparison with the spectra of nucleotides and other small oligonucleotides.[27,89] In this manner various spectral regions can be defined. In the case of DNA oligonucleotide spectra in D_2O where only the non-exchangeable protons are observed (see Fig. 7), the base H8, H6 and H2 resonances lie between 7 and 8.5 ppm, the cytosine H5 and the H1' sugar resonances between 5 and 6.5 ppm, the H3' sugar resonances between 4.5 and 5 ppm, the H4', H5' and H5" sugar resonances between 3.5 and 4.5 ppm, the H2' and H2" sugar resonances between 1.8 and 3 ppm, and the methyl protons of the thymine residues between 1.4 and 1.8 ppm. In spectra in H_2O where both exchangeable and non-exchangeable protons are observed (see Fig. 8), the exchangeable imino proton resonances lie between 12 and 14 ppm, and the exchangeable amino proton resonances between 6.5 and 8.5 ppm.

In the case of RNA oligonucleotides, the spectral dispersion of the sugar resonances is less favourable, as all the sugar resonances, with the exception of the H1' resonances, lie within a narrow region of the spectrum between 4 and 5 ppm. The other proton types resonate in the same regions as their counterparts in DNA oligonucleotides.

To complete the first level resonance assignment it is helpful to identify spin system by means of a

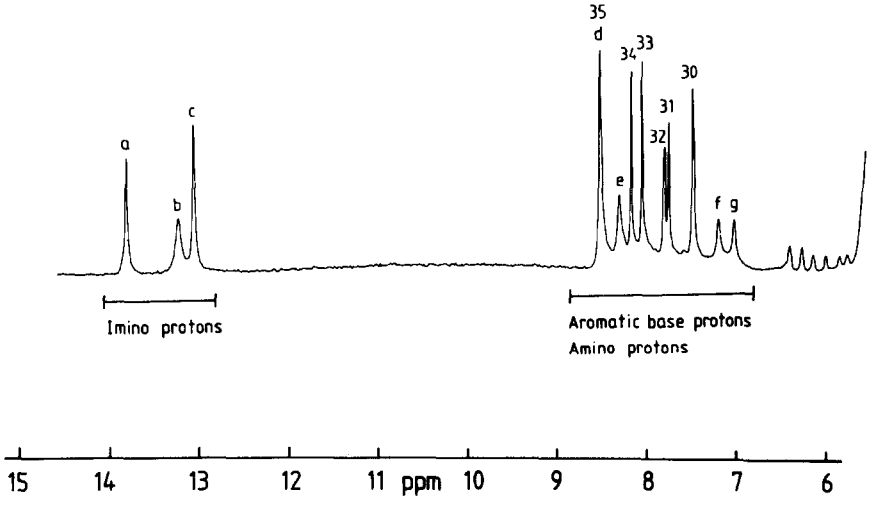

FIG. 8. 500 MHz ^{1}H-NMR spectrum between 6 and 15 ppm of the DNA hexamer 5′d(CGTACG)$_2$ in 90% H_2O at 5°C. The exchangeable proton resonances are labelled a–g and the non-exchangeable base proton resonances are labelled as in Fig. 7 (see ref. 57 for assignments). The experimental conditions are as in Fig. 7 except the sample is in 90% H_2O/10% D_2O.

2D homonuclear *J* correlated (COSY) spectrum. A summary of the COSY connectivities is shown in Fig. 9 and an example of a COSY spectrum is shown in Fig. 10 for a single stranded DNA undecamer. From the COSY spectrum the *J* connectivities between the H5 and H6 resonances of the cytosine residues and between the H6 and methyl resonances of the thymine residues (via their four bond spin–spin coupling) are easily established. In addition the sugar resonances can be grouped into

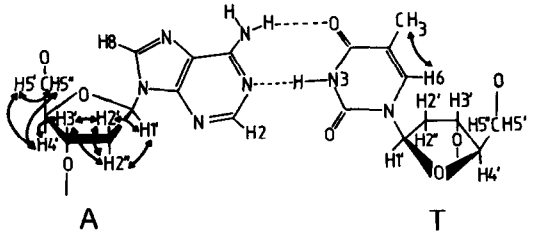

COSY CONNECTIVITIES

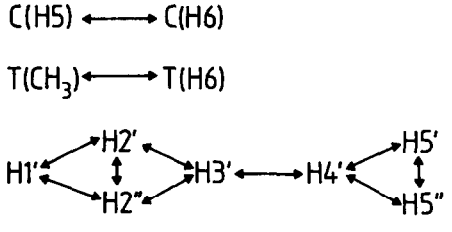

FIG. 9. Schematic representation of through bond *J* connectivities in an AT base-pair. All COSY connectivities in DNA are listed in the bottom part of the figure.

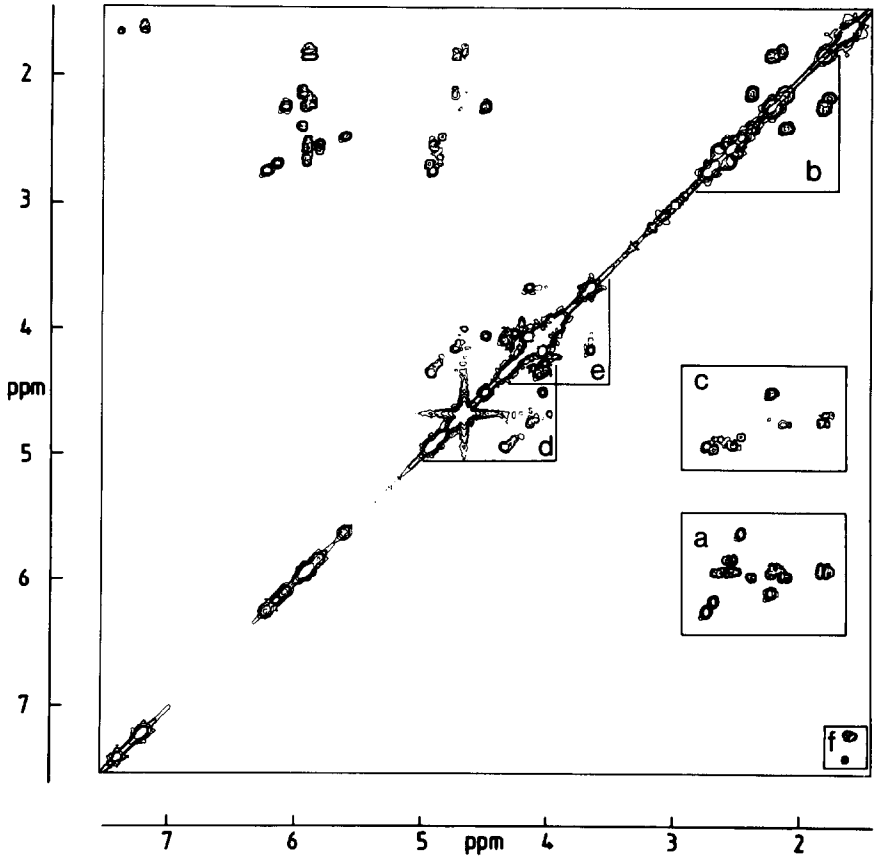

FIG. 10. 500 MH absolute value COSY spectrum of the single stranded DNA undecamer 5'd AAGTGTGATAT between 1.5 and 7.5 ppm.[112] The cross-peaks corresponding to the H1'–H2'/H2'', H2' ↔ H2'', H2'/H2'' ↔ H3', H3' ↔ H4', H4' ↔ H5'/H5'', T(H6) ↔ T(CH_3) connectivities are indicated by boxed regions marked a to f respectively. The digital resolution is 3.59 Hz/point. Experimental conditions: 6 mM single-stranded undecamer in 99.96% D_2O containing 500 mM KCl, 50 mM potassium phosphate pH* 6.8 and 0.1 mM EDTA; temperature 30°C.

families of signals belonging to the same network of coupled spins via the intranucleotide pathway H1' ↔ H2'/H2'' ↔ H3' ↔ H4' ↔ H5'/H5''. In practice, however, this is usually restricted to the H1' ↔ H2'/H2'' connectivities as the chemical shift dispersion of the H3', H4', H5' and H5'' resonances is limited.

3.2. *Sequential Resonance Assignment*

The full potential of NMR spectroscopy for structural studies can only be realized after identification of individual resonance lines. The general approach for obtaining sequential resonance assignments in ^{1}H-NMR spectra of proteins has been pioneered by Wüthrich and his collaborators.[32-37] In a similar vein, comprehensive sequential resonance assignment strategies for nucleic acids have recently been put forward independently by a number of groups based on the known structures of DNA and RNA.[54-67] These assignment strategies rely exclusively on the use of NOE measurements, either 1D or 2D, to obtain connectivities between all protons that are separated by short distances ($\lesssim$5 Å) within the spatial structure. Thus in double-stranded oligonucleotides, neighbouring bases can be identified as well as bases belonging to two different strands which are involved in base-pairing. These NOE measurements provide the main body of information necessary for

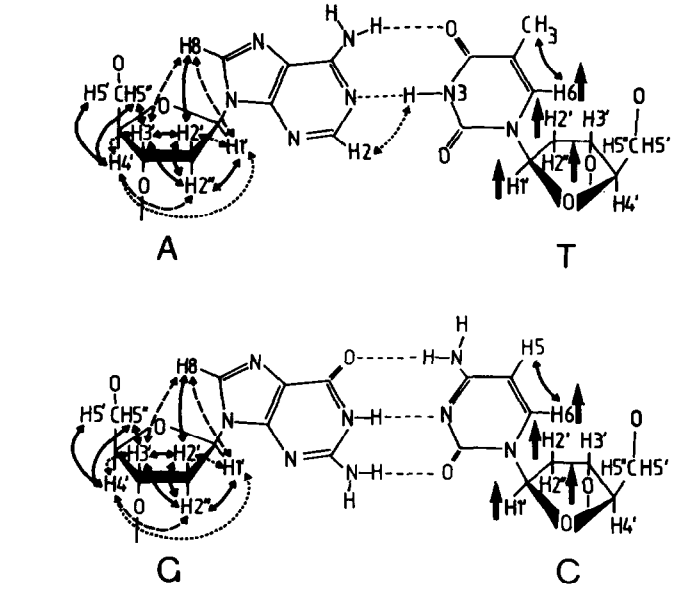

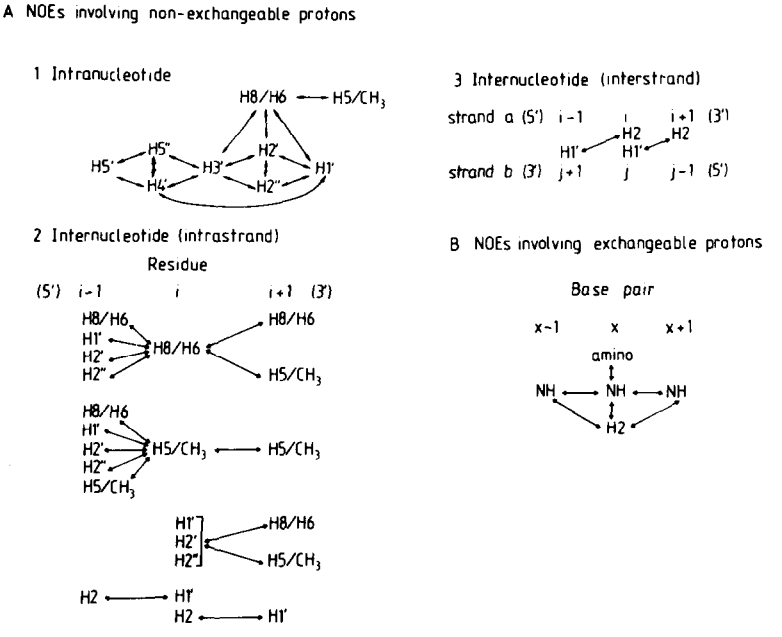

FIG. 11. Schematic representation of through space connectivities for right-handed B DNA. The intranucleotide interproton distances are represented as follows: ↔ ≤ 2.5 Å; ←– – –→ ≤ 3.5 Å; ←——→ ≤ 5 Å. Internucleotide distance relations are shown on the right-hand side with large arrows (↑) next to those protons that are separated by ≤ 5 Å from the H8, H6, H5 or methyl protons of the base on their 3′ side. All distance relationships are equally applicable to A DNA with the exception of the intranucleotide distance between the H2′ and H8/H6 protons which is larger than 3.5 Å and the intranucleotide distance between the H3′ and H8/H6 protons which is less than 3.5 Å in A DNA. The bottom part of the figure lists all interproton connectivities (distance ≤ 5 Å) which are applicable to both right-handed A and B DNA (based on crystal and fibre diffraction data given in ref. 5–11 and 16–18).

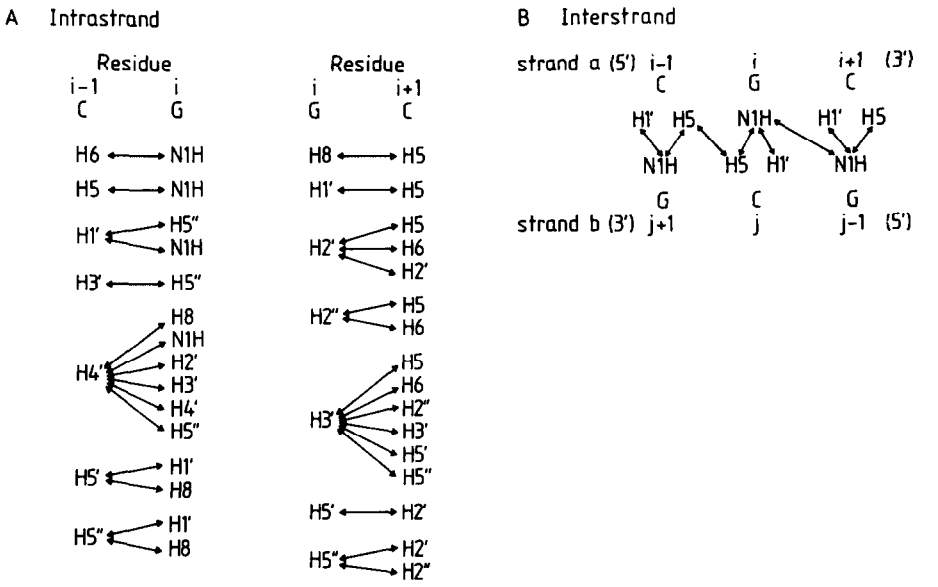

FIG. 12. Internucleotide NOE connectivities for left-handed Z-DNA (poly d(GC)). All interproton distances $\leqslant 5$ Å are listed (based on the crystal structures in ref. 12, 13).

assignment, and in cases where not all J connectivities can be resolved, will lead to virtually complete assignments in their own right. Figure 11 summarizes a comprehensive NOE strategy for the assignment of all proton resonances in right-handed single and double-stranded DNA helices. (It should be noted of course that the connectivities involving the exchangeable imino proton resonances apply only to double stranded helices.) In the case of left-handed Z DNA, the intranucleotide distance relationships are the same as those in right-handed DNA (although the relative magnitudes of the sugar–base NOEs are significantly different for the purine residues which adopt a syn conformation as opposed to the anti conformation in right-handed DNA). The internucleotide distance relationships, however, are entirely different for Z DNA and these are summarized in Fig. 12.

It is particularly important to bear in mind that the application of the schemes shown in Figs 11 and 12 for the NOE based sequential resonance assignment does not require the initial assumption of a particular helix type for the following reasons. First, the general pattern of NOEs observed for right-handed A and B type helices (see Fig. 11) is quite different from that observed for left-handed Z DNA (see Fig. 12), and is easily ascertained from a simple inspection of the complete NOE data set. This process is facilitated by the acquisition of a 2D NOE spectrum which enables one to view the entire data set in the compact form of a single contour plot. Second, the additional demands, constraints and information extracted from the J connectivities, the known nucleotide sequence, the nature of the terminal residues, and, most of all, the directionality of a large number of the internucleotide NOEs, makes the assignments based on the NOE data completely unambiguous. Furthermore, independent evidence as to the helical state of a particular oligonucleotide can always be easily ascertained from a CD spectrum. Thus *no* circular arguments are involved in the sequential assignment procedure.

3.3. *Examples of Sequential Resonance Assignment*

In the examples given below, illustrating the NOE based sequential resonance assignment strategy, the oligonucleotides all belong to the right-handed family of DNA conformations.

The 1D pre-steady NOE method of assignment is illustrated in Fig. 13 with respect to the non-exchangeable protons of residues G_2, T_3, A_4 and C_5 of the self-complementary DNA hexamer 5'd $(C_1G_2T_3A_4C_5G_6)_2$.[56,57] The selective irradiation pulse used in these measurements was applied for

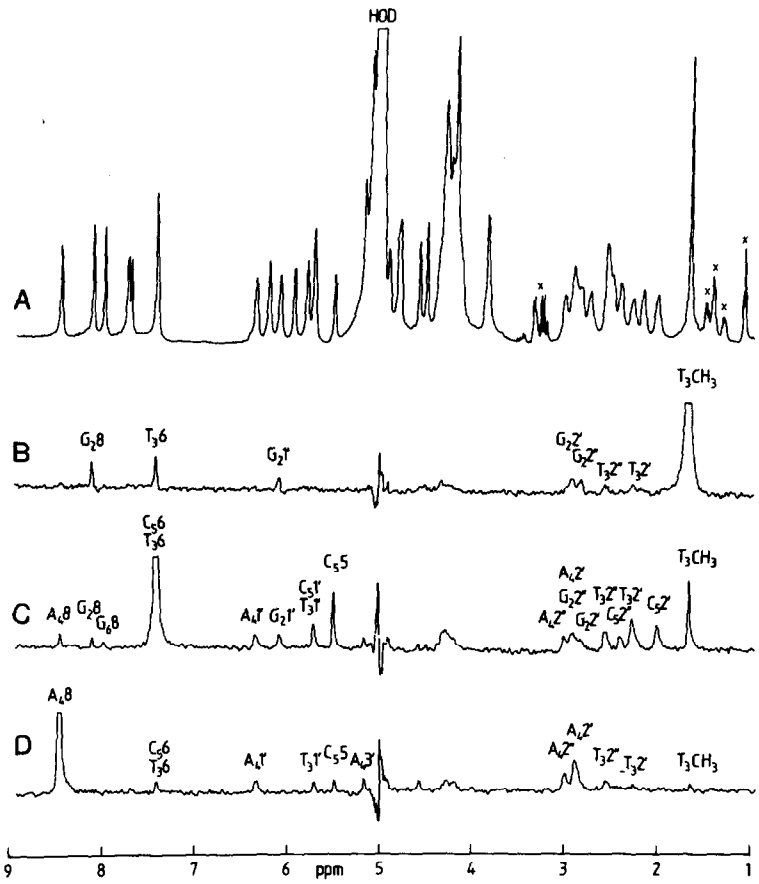

FIG. 13. Pre-steady state NOE measurements on the DNA hexamer 5'd(CGTACG)$_2$ in 99.96% D_2O at 5°C.[56] (A) The 500 MHz ^{1}H-NMR spectrum; difference spectra (off-resonance minus on-resonance pre-irradiation) following presaturation for 0.3 sec of the $T_3(CH_3)$ (B), $T_3(H6)/C_5(H6)$ (C), and $A_4(H8)$ (D) resonances. Relevant assignments are taken from ref. 57. The experimental conditions are the same as in Fig. 7. (The peaks labelled with an x are due to residual triethylammonium acetate and other impurities.)

0.3 sec, and control experiments using different irradiation times for a few selected resonances indicated that the initial rate approximation [eqn. (2)] is valid at this irradiation time. This is easily confirmed by inspection of Figs 14 and 15 which show the time dependence of some selected NOEs observed on C(H6) and H2'' resonances following irradiation of the corresponding C(H5) and H2' resonances respectively.[91] Up to 0.3 sec, the deviation from linearity is minimal. It is also worth noting that the approximation in eqn. (3) remains valid up to values of t 3 to 4 times longer than in eqn. (2). Irradiation of the $T_3(CH_3)$ resonance (Fig. 13B) results in (i) a direct intranucleotide NOE on the T_3(H6) resonance and indirect intranucleotide NOEs (via the T_3(H6) proton) on the T_3(H2') and T_3(H2'') resonances, and (ii) direct internucleotide NOEs to resonances of the 5' nucleotide, namely the G_2(H8), G_2(H1'), G_2(H2') and G_2(H2'') resonances. Irradiation of the $T_3(H6)/C_5(H6)$ resonance (Fig. 13C) results in a combination of NOEs: (i) intranucleotide NOEs between the T_3(H6) proton and the $T_3(CH_3)$, T_3(H1'), T_3(H2') protons, and between the C_5(H6) proton and the C_5(H5), C_5(H1') and C_5(H2') protons; (ii) indirect intranucleotide NOEs between the T_3(H6) and C_5(H6) protons and their respective H2'' protons via the H2' protons (which occur owing to the very small separation (1.78 Å) between the H2' and H2'' protons of the same nucleotide); and (iii) direct internucleotide NOEs between the T_3(H6) proton and the G_2(H8), G_2(H1'), G_2(H2'), G_2(H2'') and A_4(H8) protons,

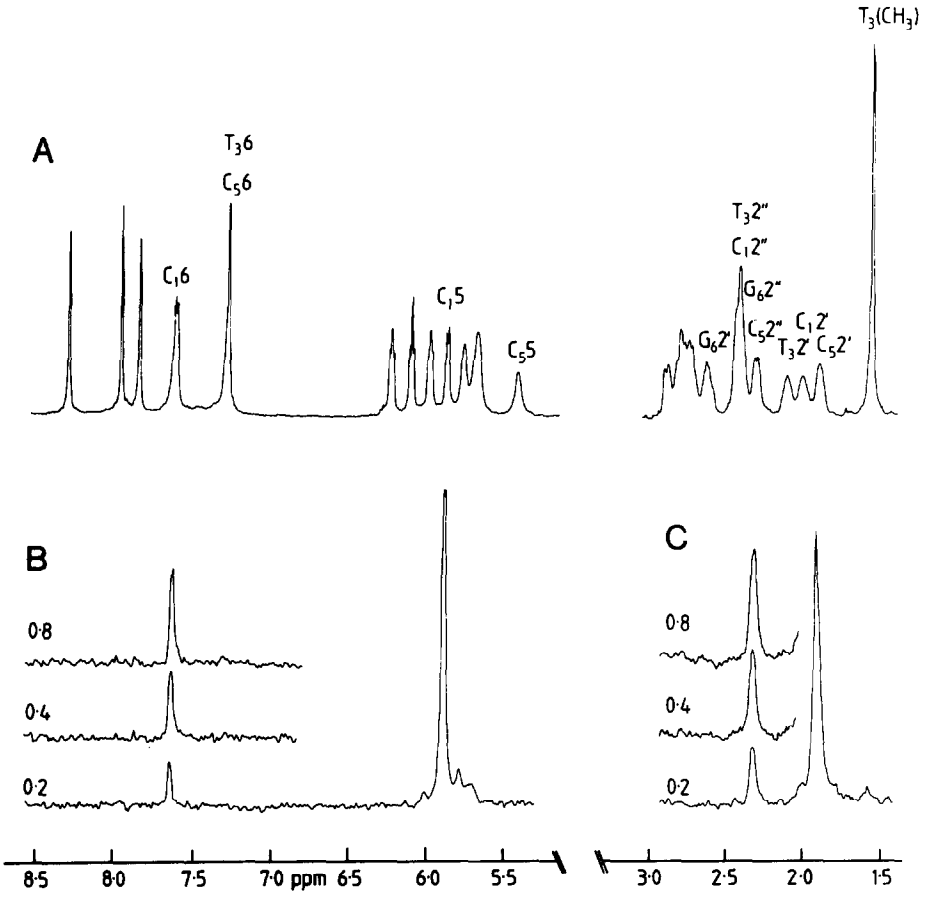

FIG. 14. (A) 500 MHz ^{1}H-NMR spectrum of the DNA hexamer 5'd(CGTACG)$_2$; (B) and (C) NOE difference spectra resulting from irradiation of the C_5(H5) and C_5(H2') resonances respectively for 0.2, 0.4 and 0.8 sec.[91] Relevant assignments are taken from ref. 57. The temperature is 23°C. Experimental conditions: 3.1 mM duplex in 99.96% D_2O containing 1 M KCl, 50 mM potassium phosphate pH* 6.5 and 0.1 mM EDTA.

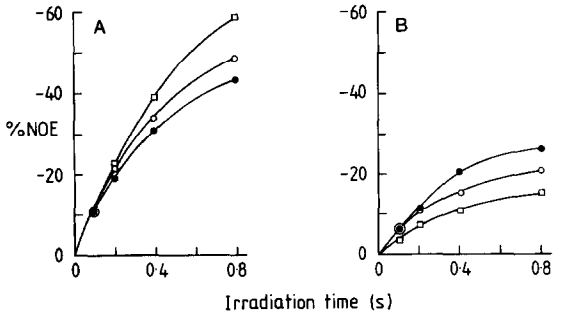

FIG. 15. Magnitude of NOEs as a function of irradiation time for the DNA hexamer 5'd(CGTACG)$_2$ at 23°C[91] (A) H2'' resonances of C_1 (●), C_5 (○) and T_3 (□) following irradiation of their respective H2' resonances. (B) H6 resonances of C_1 (●), C_5 (○) and T_3 (□) following irradiation of the C_1(H5), C_5(H5) and T_3(CH_3) resonances. The experimental conditions are as in Fig. 14.

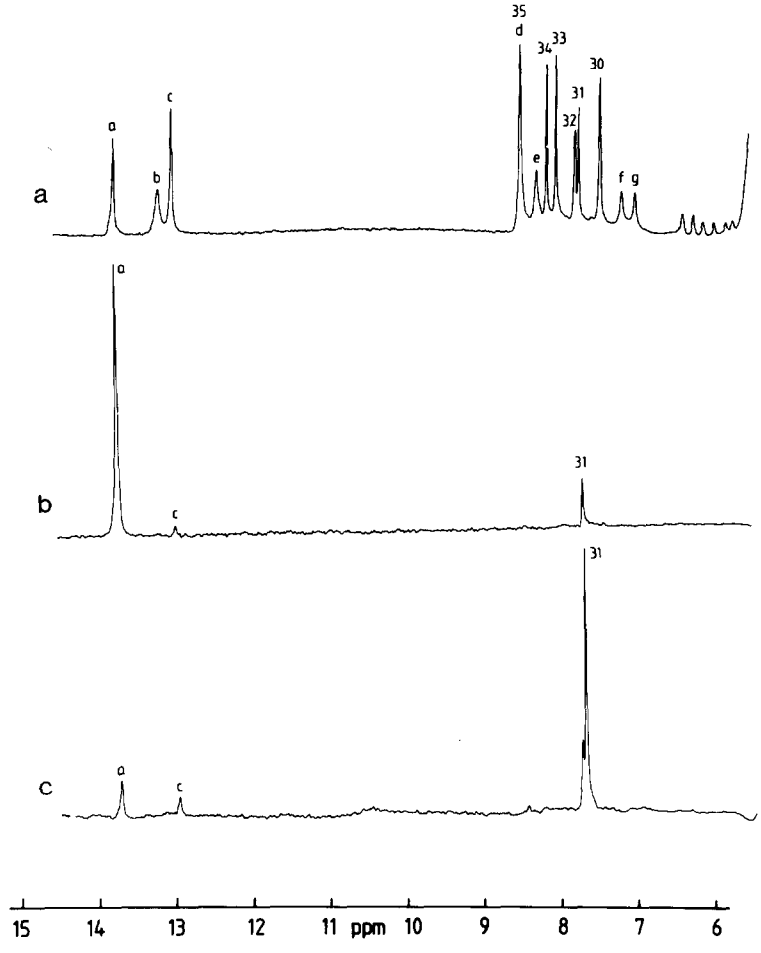

FIG. 16. Pre-steady state NOE measurements on double-stranded 5'd(CGTACG)$_2$ in 90% H_2O at 5°C (57). (a) The 500 MHz ^{1}H-NMR spectrum between 6 and 15 ppm. Difference spectra (off resonance minus on-resonance pre-irradiation) following presaturation for 0.3 sec of (b) the T_3(H3) imino proton resonance (peak a) at 13.75 ppm, and (c) the A_4(H2) proton resonance (peak 31) at 7.70 ppm. The other peak seen in the difference spectra, peak c, is the G_2(H1) imino proton resonance. The experimental conditions are as in Fig. 8.

and between the C_5(H6) proton and the A_4(H8), A_4(H1'), A_4(H2') and A_4(H2'') protons. Irradiation of the A_4(H8) resonance (Fig. 13D) then results in (i) direct intranucleotide NOEs on the A_4(H1'), A_4(H2') and A_4(H3') resonances and an indirect intranucleotide NOE (via the A_4(H2') proton) on the A_4(H2'') resonance; (ii) direct internucleotide NOEs on resonances of the 5' nucleotide, namely the T_3(H6), T_3(CH_3), T_3(H1'), T_3(H2') and T_3(H2'') resonances; and (iii) direct internucleotide NOEs on resonances of the 3' nucleotide, namely the C_5(H5) and C_5(H6) resonances.

The same procedure can be applied to the exchangeable imino protons as illustrated in Fig. 16 for 5'd(CGTACG)$_2$.[57] Thus irradiation of the imino proton resonance peak a (Fig. 16b) results in a large intrabase pair NOE on the A_4(H2) proton resonance (peak 31) and a small interbase pair NOE on the imino proton resonance peak c. Therefore peak a must be the T_3(H3) proton, peak c the G_2(H1) proton and, by exclusion, peak b the G_6(H1) proton. This is confirmed by irradiating the A_4(H2) proton resonance (peak 31) which results in an intrabase-pair NOE on the T_3(H3) imino proton resonance and an interbase-pair NOE on the G_2(H1) imino proton resonance c (Fig. 16c).

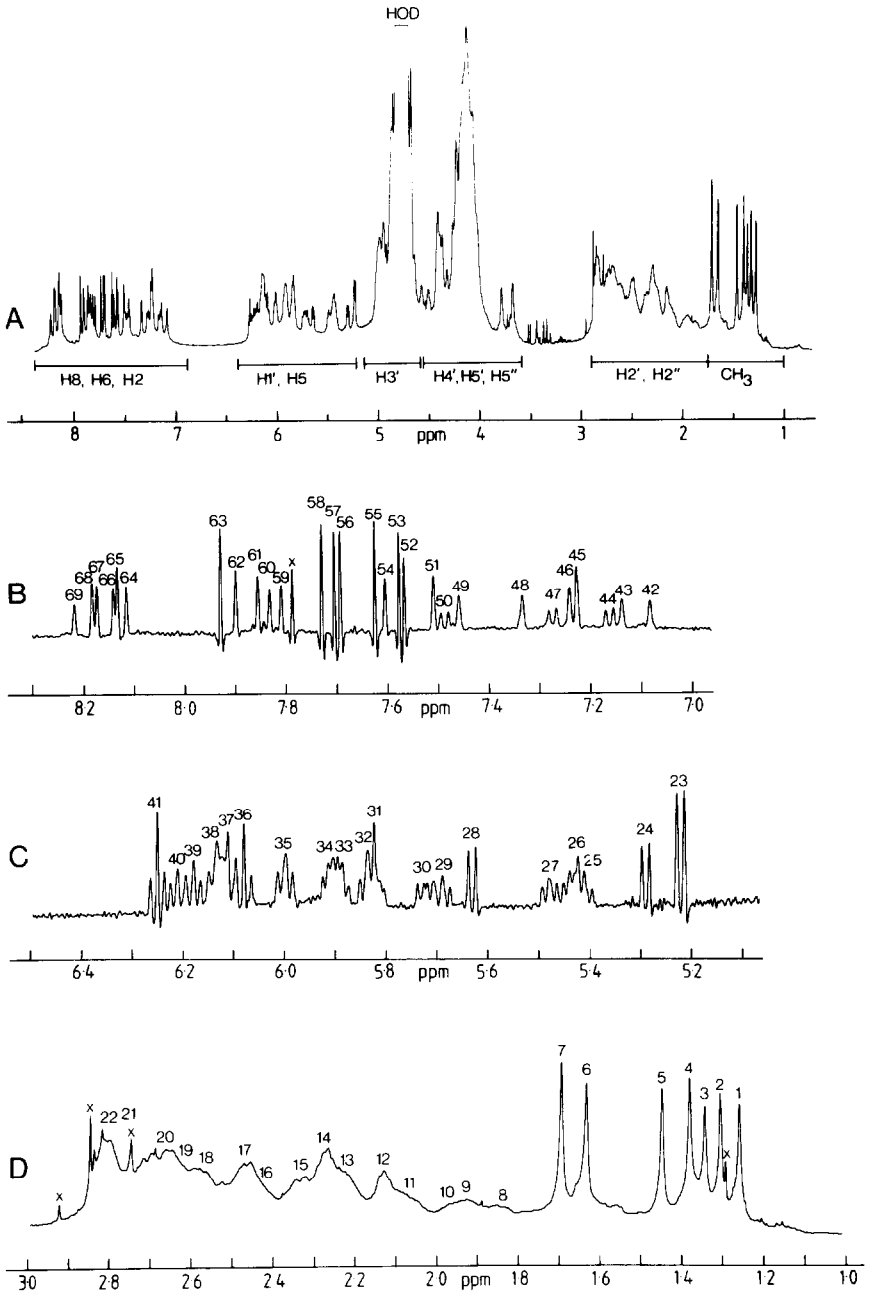

FIG. 17. 500 MHz ^{1}H-NMR spectrum of the duplex undecamer [5'd(AAGTGTGACAT)·5'd (ATGTCACACTT)] in 99.96% D_2O at 23°C. (A) Complete spectrum between 1.0 and 8.5 ppm. (B) Resolution enhanced expansion of the H8/H6/H2 resonance region between 7.0 and 8.3 ppm. (C) Resolution enhanced expansion of the H1'/H5 resonance region between 5.1 and 6.5 ppm. (D) Expansion of the CH_3 and H2'/H2" resonance regions between 1.0 and 3.0 ppm. The assignments of the numbered resonances are given in ref. 58. Experimental conditions: 2 mM duplex 11mer in 99.96% D_2O containing 300 mM KCl, 15 mM potassium phosphate pH* 6.8 and 0.18 mM EDTA. The peaks marked x arise from low molecular weight impurities. The expansions shown in (B) and (C) were resolution enhanced by multiplying the free induction decay by a two term exponential function (Lorentz–Gauss multiplication) prior to Fourier transformation.

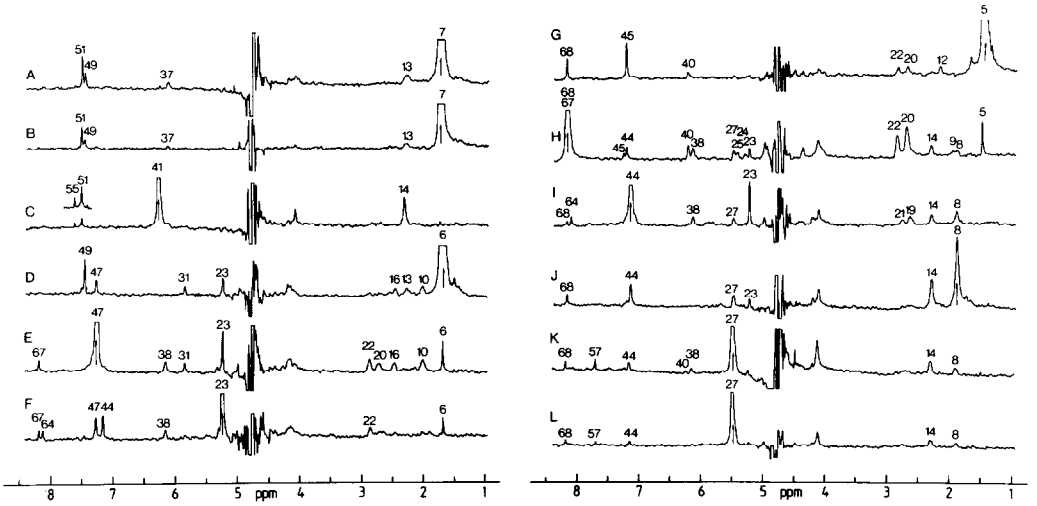

FIG. 18. 500 MHz ^{1}H pre-steady state NOE difference spectra (off-resonance minus on-resonance irradiation) on the duplex undecamer [5′d(AAGTGTGACAT)·5′d(ATGTCACACTT)] in 99.96% D_2O at 23°C[58] following irradiation of: (A) and (B) the $T_{11B}(CH_3)$ resonance 7; (C) the $T_{11B}(H1')$ resonance 41; (D) the $T_{10B}(CH_3)$ resonance 6; (E) the $C_{9B}(H6)$ resonance 47; (F) the $C_{9B}(H5)/C_{9A}(H5)$ resonance 23; (G) the $T_{11A}(CH_3)$ resonance 5; (H) the $A_{10A}(H8)$ and $A_{8B}(H8)$ resonances, 68 and 67; (I) the $C_{9A}(H6)$ resonance 44; (J) the $C_{9A}(H2')$ resonance 8; and (K) and (L) the $C_{9A}(H1')$ resonance 27. See text for the assignments of the other peaks seen in the difference spectra. Note that a decrease in intensity of a particular resonance is seen as a positive peak in the difference spectrum. The irradiating pulse was applied for 0.8 sec for all NOE difference spectra with the exception of (B) and (L) where it was applied for 0.4 sec. The experimental conditions are the same as in Fig. 17.

The 1D NOE approach can also be successfully applied to larger oligonucleotides. This is illustrated for the non-self-complementary DNA undecamer[58]:

5′d $(A_1\ A_2\ G_3\ T_4\ G_5\ T_6\ G_7\ A_8\ C_9\ A_{10}\ T_{11})$ 3′ A strand

3′d $(T_{11}\ T_{10}\ C_9\ A_8\ C_7\ A_6\ C_5\ T_4\ G_3\ T_2\ A_1)$ 5′ B strand

The 500 MHz ^{1}H-NMR spectrum of this oligonucleotide and some examples of pre-steady state NOE difference spectra in D_2O are shown in Figs 17 and 18, respectively.

Considering the B strand first, we note that the sequence CTT of the three terminal residues is unique in the duplex, thereby giving one an easy entry into the sequential assignment of the B strand resonances via the well resolved methyl proton resonances. Irradiation of the $T(CH_3)$ resonance 7 (Fig. 18A) results in NOEs on two T(H6) resonances (peaks 51 and 49), an H1′ resonance (peak 37) and an H2′/H2″ resonance (peak 13). The magnitude of the NOE on peak 51 is $\sim -20\%$ whilst that on peak 49 is $\sim -10\%$. Given that there is only a single occurrence of a TT sequence and that, in the case of right-handed DNA, irradiation of a $T(CH_3)$ resonance will give rise to a large intranucleotide NOE on a T(H6) resonance, and smaller internucleotide NOEs on the H8/H6, H1′, H2′ and H2″ resonances of the 5′ residue, immediately enables one to assign peaks 7 and 15 to the CH_3 and H6 protons respectively of T_{11B}, and peaks 49, 37 and 13 to the H6, H1′ and H2′/H2″ protons respectively of T_{10B}. The identification of the H1′, H2′ and H2″ resonances of T_{11B} can be achieved by irradiation of the T_{11B} (H6) resonance 51 (spectrum not shown) which results in intranucleotide NOEs on the $T_{11B}(CH_3)$ (peak 7), $T_{11B}(H1')$ (peak 41) and $T_{11B}(H2'/H2'')$ (peak 14) resonances, and in the same internucleotide NOEs as observed on irradiation of the $T_{11B}(CH_3)$ resonance. Irradiation of the $T_{11B}(H1')$ resonance 41 (Fig. 18C) confirms the assignment of the $T_{11B}(H6)$ and $T_{11B}(H2'/H2'')$ resonances by giving rise to the expected intranucleotide NOEs on these resonances, and, in addition, results in a very small interstrand NOE on the $A_{2A}(H2)$ resonance (peak 55). The $T_{10B}(CH_3)$ resonance is easily assigned to peak 6 by the large intranucleotide NOE observed on irradiation of the $T_{10B}(H6)$ resonance 49 (spectrum not shown). Irradiation of the $T_{10B}(CH_3)$ resonance 6 (Fig. 18D)

gives rise to the expected large intranucleotide NOE on the T_{10B}(H6) resonance (peak 49), to an indirect intranucleotide NOE via the T_{10B}(H6) proton on the T_{10B}(H2′)/(H2″) resonance (peak 13), and to internucleotide NOEs on the H6 (peak 47), H5 (peak 23), H1′ (peak 31), H2′ (peak 10) and H2″ (peak 16) resonances of the residue on its 5′ side, C_{9B}. Irradiation of the C_{9B}(H6) resonance peak 47 (Fig. 18E) then results in intranucleotide NOEs on the C_{9B}(H5) (peak 23), C_{9B}(H1′) (peak 31), C_{9B}(H2′) (peak 10) and C_{9B}(H2″) (peak 16) (indirect via C_{9B}(H2′) proton) resonances, an internucleotide NOE on the CH_3 resonance (peak 6) of the 3′ residue T_{10B}, and internucleotide NOEs on the H8 (peak 67), H1′ (peak 38), H2′ (peak 20) and H2″ (peak 22) resonances of the 5′ residue of A_{8B}. The internucleotide NOEs on the H8, H1′ and H2″ resonances of A_{8B} and the CH_3 resonance of T_{10B} are also observed on irradiation of the C_{9B}(H5) resonance 23 (Fig. 18F). (Note that peak 23 also contains the C_{9A}(H5) resonance).

The same approach can be used to assign sequentially the A strand resonances, and, as in the case of the B strand, the sequence CAT of the three terminal residues is unique in the duplex, thereby simplifying matters. Irradiation of the $T_{11A}(CH_3)$ resonance 5 (Fig. 18G) results in a large intranucleotide NOE on the T_{11A}(H6) resonance (peak 45), an indirect intranucleotide NOE via the T_{11A}(H6) proton on the T_{11A}(H2′)/(H2″) resonance (peak 12), and internucleotide NOEs on the H8 (peak 68), H1′ (peak 40), H2′ (peak 20) and H2″ (peak 22) resonances of the residue on its 5′ side, A_{10A}. Irradiation of the A_{10A}(H8) resonance alone is not feasible as peak 68 closely overlaps with peak 67, the A_{8B}(H8) resonance. Thus, irradiation of peak 67/68 (Fig. 18H) results in a combination of NOEs arising from both the A_{10A}(H8) and A_{8B}(H8) resonances. From the A_{10A}(H8) proton there are intranucleotide NOEs on the A_{10A}(H1′) (peak 40), A_{10A}(H2′) (peak 20) and A_{10A}(H2″) (peak 22) (indirect via A_{10A}(H2′) proton) resonances, an internucleotide NOE on the CH_3 resonance (peak 5) of the 3′ residue T_{11A}, and internucleotide NOEs on the H6 (peak 44), H5 (peak 23), H1′ (peak 27), H2′ (peak 8) and H2″ (peak 14) resonances of the 5′ residue C_{9A}. (The NOEs arising from the A_{8B}(H8)

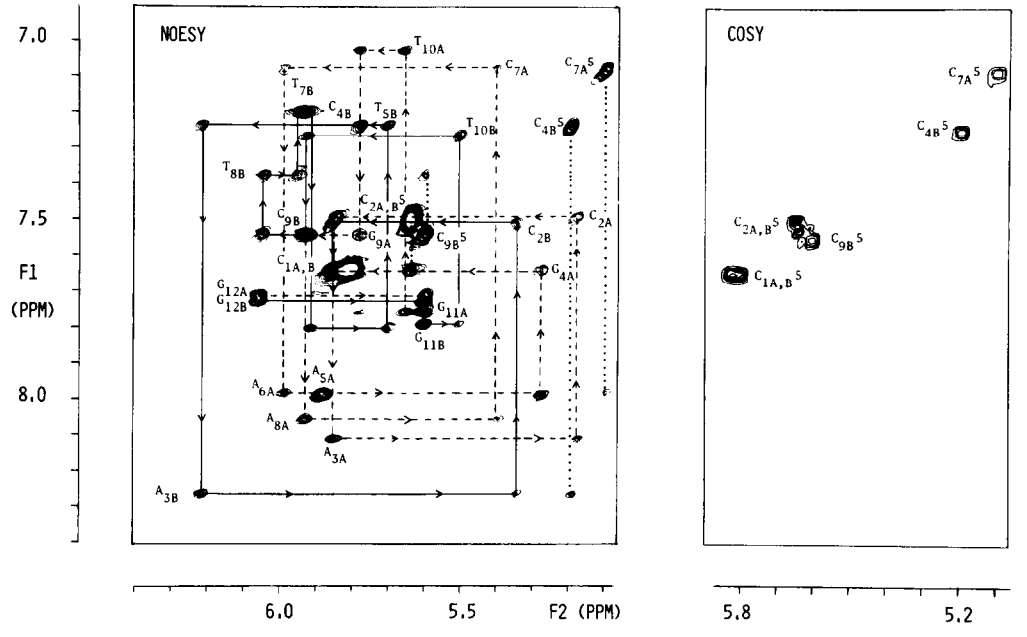

FIG. 19. H8/H6 (F1 axis)–H1′/H5(F2 axis) region of the pure absorption phase NOESY (300 msec mixing time) and absolute value COSY spectra of the duplex dodecamer [5′d(CCAGAACAGTGG)·5′d(CCACTGTTCTGG)] in 99.96% D_2O at 25°C (92). The H1′(i-1) ↔ H8/H6(i) ↔ H1′(i) NOE connectivities are represented by interrupted (– – –) and continuous (———) lines for the A and B strands respectively. The H8/H6 (i-1)-H5(i) NOE connectivities are indicated by the dotted lines (·····). The H1′ and C(H5) protons are indicated as X_i and C_i5 respectively in the figure. Experimental conditions: 8 mM duplex in 99.96% D_2O containing 100 mM KCl, 10 mM potassium phosphate pH* 6.8 and 0.02 mM EDTA. The digital resolution is 3.9 Hz/point.

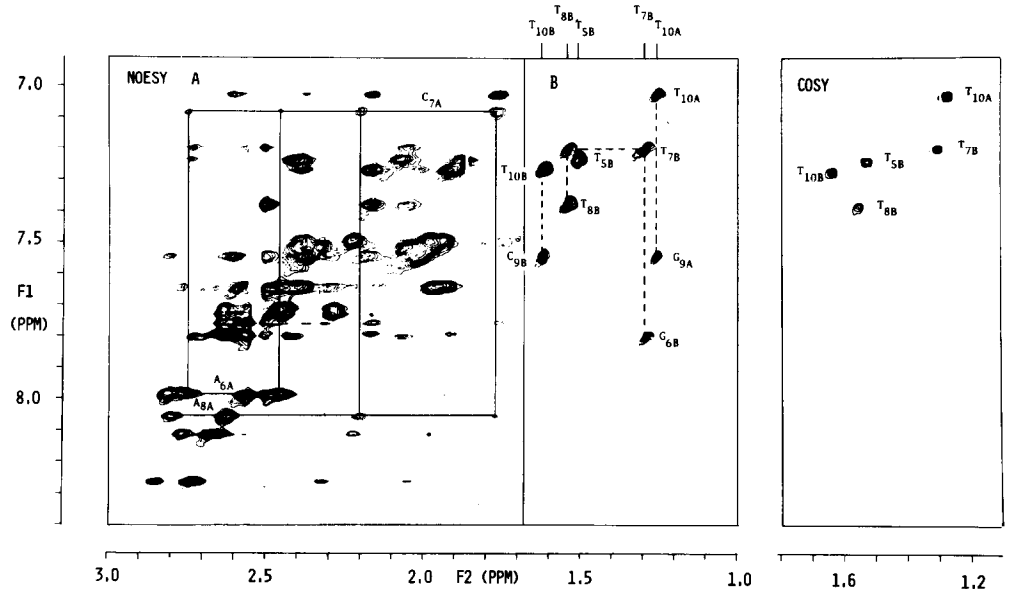

FIG. 20. (A) H8/H6 (F1 axis)–H2′/H2″(F2 axis) and (B) H8/H6(F1 axis)–CH_3 (F2 axis) regions of the pure phase absorption NOESY spectrum (300 msec mixing time) of the dodecamer [5′d(CCAGAACAGTGG)·5′d (CCACTGTTCTGG)] in 99.96% D_2O at 25°C.[92] An absolute value COSY spectrum of the H8/H6 (F1 axis)–CH_3(F2 axis) is also shown. An example of the H2′/H2″(i-1) ↔ H8/H6(i) ↔ H2′/H2″(i) NOE connectivities is indicated by the continuous line (———) for the A_{6A}–C_{7A}–A_{8A} sequence of the A chain. The interrupted lines (– – –) in (B) indicate H8/H6(i-1)–CH_3(i) NOE connectivities. The assignments by the side of the cross peaks in (B) refer to the F1 axis. The experimental conditions are as in Fig. 19.

proton are as follows: intranucleotide NOEs on the A_{8B}(H1′) (peak 38), A_{8B}(H2′) (peak 20) and A_{8B}(H2″) (peak 22) resonances, and internucleotide NOEs on the C_{7B}(H6) (peak 45), C_{7B}(H5) (peak 24), C_{7B}(H1′) (peak 25), C_{7B}(H2′) (peak 9) and C_{7B}(H2″) (peak 14) resonances.) Irradiation of the C_{9A}(H6) resonance 44 (Fig. 41) results in intranucleotide NOEs on the C_{9A}(H5) (peak 23), C_{9A}(H1′) (peak 27), C_{9A}(H2′) (peak 8), C_{9A}(H2″) (peak 14) (indirect via C_{9A}(H2′) proton) and C_{9A}(H3′) (4.98 ppm) resonances, an internucleotide NOE on the H8 resonance (peak 68) of the 3′ residue A_{10A}, and internucleotide NOEs on the H8 (peak 64), H1′ (peak 38), H2′ (peak 19) and H2″ (peak 21) resonances of the 5′ residue A_{8A}. (The internucleotide NOEs on the H8 and H1′ resonances of the A_{8A} residue are also observed on irradiation of the C_{9A}(H5) resonance 23; see Fig. 18F). Fig. 18J illustrates the NOEs observed on irradiation of the C_{9A}(H2′) resonance 8: there are direct intranucleotide NOEs on the C_{9A}(H2″) (peak 14), C_{9A}(H1′) (peak 27) and C_{9A}(H6) (peak 44) resonances, a small indirect intranucleotide NOE via the C_{9A}(H6) proton on the C_{9A}(H5) resonance (peak 23), and an internucleotide NOE on the H8 resonance (peak 68) of the 3′ residue A_{10A}. These findings are confirmed by irradiation of the C_{9A}(H1′) resonance 27 (Fig. 18K) which results in intranucleotide NOEs on the C_{9A}(H6) (peak 44), C_{9A}(H2′) (peak 8) and C_{9A}(H2″) (peak 14) resonances, internucleotide NOEs on the H8 (peak 68) and H1′ (peak 40) resonances of the 3′ residue A_{10A}, and internucleotide NOEs on the H1′ (peak 38) and the H2 (peak 57) resonances of the 5′ residue A_{8A}.

The approach used for the interpretation of the 2D NOE experiment is identical to that described above. This is illustrated in Figs 19 and 20 which show the H8/H6(F1)–H1′/H5(F2) and H8/H6(F1)–H2′–H2″/CH_3(F2) regions respectively of the pure phase absorption NOESY spectrum in D_2O of the non self-complementary DNA dodecamer (92):

5′d (C_1 C_2 A_3 G_4 A_5 A_6 C_7 A_8 G_9 T_{10} G_{11} G_{12}) 3′ A strand

3′d (G_{12} G_{11} T_{10} C_9 T_8 T_7 G_6 T_5 C_4 A_3 C_2 C_1) 5′ B strand

Considering the B chain as an example, we note that the sequence $G_{6B}T_{7B}T_{8B}$ is unique in the duplex dodecamer. Examination of the NOESY spectrum in Fig. 20B immediately establishes the assignment

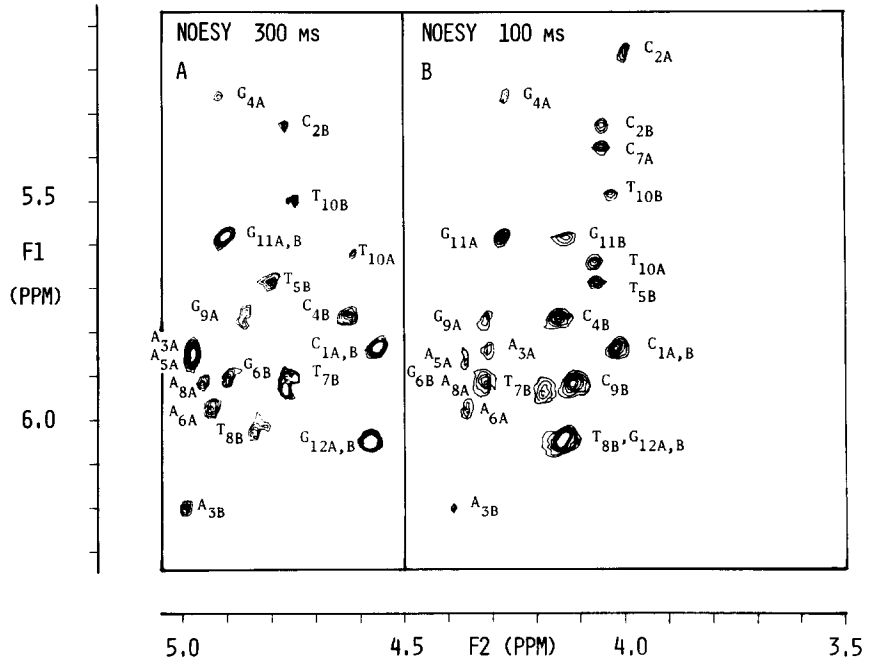

FIG. 21. (A) H1′(F1 axis)–H3′(F2 axis) and (B) H1′(F1 axis)–H4′(F2 axis) regions of the pure phase absorption NOESY spectrum of the dodecamer [5′d(CCAGAACAGTGG)·5′d(CCACTGTTCTGG)] with mixing times of 300 and 100 msec respectively.[92] The experimental conditions are as in Fig. 19.

of the methyl and base protons of these three residues via the NOE pathway

$$G_{6B}(H8) \leftrightarrow T_{7B}(CH_3) \leftrightarrow T_{7B}(H6) \leftrightarrow T_{8B}(CH_3) \leftrightarrow T_{8B}(H6)$$

With this knowledge in mind, one need only turn to the NOESY spectra in Figs 19 and 20A to establish NOE connectivities between the H8/H6 and H1′ protons and between the H8/H6 and H2′/H2″ protons, respectively, of these residues, thereby providing a useful starting point with which to extend the assignment of the B chain H8/H6 and H1′, H2′/H2″ protons in both directions. Once these assignments are in hand the relevant intranucleotide NOEs can be used to assign the other sugar proton resonances, as illustrated in Fig. 21 with respect to the H3′ and H4′ resonances.

It will be noted that in the descriptions given above a distinction is made between the H2′ and H2″ sugar resonances. This is readily made on the basis of two criteria. First the intranucleotide NOE between the H8/H6 and H2′ protons is always larger than that between the H8/H6 and H2″ protons for all glycosidic bond torsion angles within the anti range characteristic of right handed B and A DNA (e.g. see Figs 13C,D, 18E,H,I and 22A); moreover, within this conformational range, the principal contribution to the observed intranucleotide NOE between the H8/H6 and H2″ protons arises from indirect cross-relaxation via the H2′ proton due to the very short separation of only 1.78 Å between the H2′ and H2″ protons. Second, the intranucleotide NOE between the H1′ and H2″ protons is usually larger and can never be smaller than that between the H1′ and H2′ protons for all sugar pucker conformations (e.g. see Figs 18K,L and 22B).

4. THREE DIMENSIONAL SOLUTION STRUCTURE DETERMINATION

4.1. *Low Resolution Structure*

Because of the r^{-6} dependence of the pre-steady state NOE, the relative magnitude of the NOEs provides a sensitive probe which can be used to obtain a qualitative view of the solution structures of short oligonucleotides.

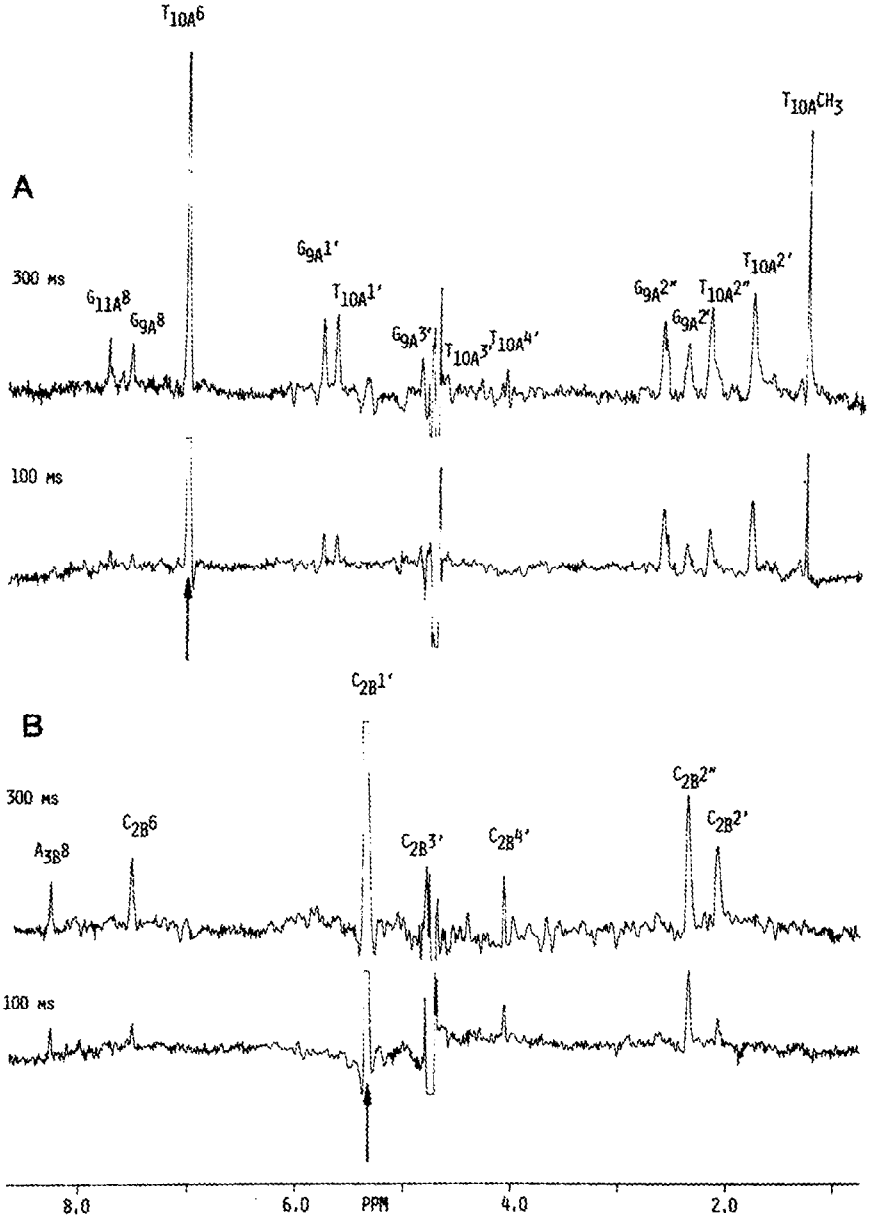

FIG. 22. Cross-section of the pure phase absorption NOESY spectra (100 and 300 msec mixing times) of the dodecamer [5'd(CCAGAACAGTGG)·5'd(CCACTGTTCTGG)] taken with (A) the T_{10A}(H6) resonance and (B) the C_{2B}(H1') resonance at the position of the diagonal.[92] These cross-sections correspond to NOE difference spectra that would be observed in conventional one-dimensional spectroscopy upon irradiation of the T_{10A}(H6) and C_{2B}(H1') resonances. The experimental conditions are as in Fig. 19.

The glycosidic bond and sugar pucker conformations can be assessed qualitatively on the basis of the relative magnitudes of the intranucleotide sugar-base NOEs. Thus, in B DNA where the glycosidic bond conformation lies in the conventional anti range with $\chi \sim -115 \pm 30°$ (IUPAC Nomenclature used) and the sugar pucker conformation extends from O1'-endo (δ(C4'–C3') ~ 100°) to C2'-endo ($\delta \sim 140°$),[6] the pattern of NOE intensities observed is $N_{H2'-H8/H6} \gg N_{H1'-H8/H6} \gtrsim N_{H3'-H8/H6}$. A

DNA, on the other hand, has a low anti glycosidic bond conformation ($\chi \sim -160 \pm 10°$) and a 3′-endo sugar pucker ($\delta \sim 80°$)[9,11] and the corresponding pattern of NOE intensities is $N_{H3'-H8/H6} \gg N_{H1'-H8/H6} \sim N_{H2'-H8/H6}$. In Z DNA, which occurs in alternating pyrimidine-purine sequences, the pyrimidine residues have essentially the same glycosidic bond and sugar pucker conformations as in B DNA and will therefore exhibit the same pattern of intranucleotide NOEs; in contrast, the purine residues have a syn conformation about the glycosidic bond ($\chi \sim 60$–$70°$) and a 3′-endo sugar pucker ($\delta \sim 80°$) so that the observed pattern of NOEs is $N_{H1'-H8/H6} \gg N_{H2''-H8/H6} \sim N_{H2'-H8/H6} \gg N_{H3'-H8/H6}$.

The handedness of the helix and the overall helical conformation can be deduced from the internucleotide NOEs with directional specificity. Thus for right-handed helices, internucleotide NOEs are observed between the H1′, H2′ and H2″ sugar proton of a given residue and the H8/H6 base proton of the adjacent 3′ but not 5′ residue and, similarly between the $T(CH_3)$ protons of a given residue and the H8/H6 proton of the adjacent 5′ but not 3′ residue. The distinction between the A and B type geometries can then be made on the basis of the relative magnitudes of the intra- and internucleotides between the H8/H6 and H2′/H2″ protons. In B DNA the observed relative intensities are $N_{H2'(i)-H8/H6(i)} \gg N_{H2''(i-1)-H8/H6(i)} > N_{H2'(i-1)-H8/H6(i)}$, whereas in A DNA they are $N_{H2'(i-1)-H8/H6(i)} \gg N_{H2''(i-1)-H8/H6(i)} > N_{H2'(i)-H8/H6(i)}$. The pattern of internucleotide NOEs observed for left-handed Z DNA is entirely different as can be seen by a comparison of Figs 11 and 12.

4.2. *Interproton Distance Determination*

In addition to providing assignments and low resolution structural information by demonstrating the proximity of two protons in space, presteady state NOE measurements allow one to determine interproton distances using eqn. (2) providing a reference distance is known and the correlation time of the unknown interproton distance vector is the same as that of the reference. In the case of DNA oligonucleotides there are three intranucleotide reference distances which are completely independent of the structure of the DNA: namely $r_{H2'-H2''}$, $r_{C(H6)-C(H5)}$ and $r_{T(H6)-T(CH_3)}$ which, on the basis of standard bond lengths and angles, have values of 1.78, 2.46 and 2.70 Å, respectively. (Note that the latter distance is an average given by $(\langle r_{ij}^{-6} \rangle)^{-1/6}$ calculated on the assumption of free rotation of the methyl group). In addition, the distance between the T(H3) and A(H2) protons in a standard Watson–Crick AT base-pair is 2.9 Å; although this distance will not be affected by propellor twisting, it will be dependent on deviations from idealized hydrogen bond length and geometry. The difficulty, therefore, lies in making the appropriate choice of reference distance in the calculations of the unknown interproton distances, particularly as it is known from relaxation studies on long pieces of DNA that the correlation time of the sugar ring is shorter than that of the bases.[93–98] Fortunately, this choice can be based on, (i) stereochemical considerations taking into account the expected ranges of the various interproton distances and the types of motions of the different protons as deduced from the analysis of X-ray thermal factors[99] and molecular dynamics calculations,[101–103] and (ii) the measured cross-relaxation rates for the H2′–H2″, C(H5)–C(H6) and $T(CH_3)$–T(H6) vectors in short oligonucleotides.[91] The latter study has shown that only a small variation occurs in the cross-relaxation rates of these interproton vectors in different residues within each oligonucleotide, and that the mean apparent correlation times of the C(H5)–C(H6) and $T(CH_3)$–T(H6) vectors are approximately equal (the contribution from free rotation of the methyl group to the apparent correlation time of the $T(CH_3)$–T(H6) vector being negligible*) and significantly greater than that of the H2′–H2″ vectors. On this basis we have assumed in our studies[56,57,103] that: (i) the correlation times for the sugar–sugar, sugar–base (with the exception of the H1′ sugar–base) and sugar–methyl interproton vectors are the same as those of the intranucleotide H2′–H2″ vector; and (ii) the correlation times for the base–base, base–methyl and H1′ sugar–base proton vectors are the same as those of the intranucleotide H5–H6 vector. These assumptions seem perfectly reasonable as one would expect that

* The reason that rotation of the methyl protons makes only a negligible contribution to the apparent correlation time of the $T(CH_3)$–H vector is as follows. As the distance between proton H and the methyl protons increases, the angle through which the H–methyl H dipolar vectors fluctuates decreases. Moreover, there is a decrease in the dipolar interaction due to the increasing distance. The combination of these two effects makes rotation of the methyl group very ineffective in the relaxation process.[116]

the contributions from internal motion to the effective correlation time to be dominated by motions within the sugar ring in case (i) and by motion about the glycosidic bond in case (ii). A check on the validity of assumption (i) can be made by calculating the intranucleotide H1′–H2″ and H2′–H3′ distances using the intranucleotide H2′–H2″ NOE and distance as a reference. Both the H1′–H2″ and H2′–H3′ distances have values of 2.3 ± 0.2 Å for all sugar puckers, and in all cases the distances calculated from the NOE data in this manner fall within this range.[57,104] Similarly, a check on the validity of assumption (ii) can be made by calculating the intranucleotide T(CH_3)–T(H6) distance and the intrabase-pair distance between the T(H3) and A(H2) protons of an AT base-pair using the H5–H6 NOE and distance as a reference: in all cases this leads to values within ± 0.1 Å of the idealized values.[57,59,60,104] The effect of choosing an inappropriate reference distance can be seen by calculating the intranucleotide H5–H6 distance using the H2′–H2″ NOE and distance as reference: this leads to a value which is ~ 0.3 Å shorter than the idealized value.

In the case of the four B type DNA oligonucleotides on which this approach has been used, the overall root mean square difference between the NMR distances and those derived from fibre diffraction data on B DNA is $\lesssim 0.5$ Å.[57,59,104]

4.3. *High Resolution Structure*

Because of the limited degrees of freedom available for a double-stranded oligonucleotide one would expect that a reasonably large number of interproton distances (around 100 for a self-complementary hexamer) would be sufficient to determine its three-dimensional solution structure with a high degree of confidence. In principle, these structures can be solved by manual model building using either skeletal models or models constructed with computer building programs. This is the approach we have used to date, and, indeed, it permits reasonably accurate values for the glycosidic (χ) and C4′–C3′ (δ) bond torsion angles to be obtained.[56,57,104] However, because of potential cumulative errors inherent in the manual approach, only qualitative information can be deduced for the other structural parameters, namely the backbone torsion angles, helical twist, helical rise and base tilt.

The problems inherent in the manual approach can potentially be overcome in three different ways. The first method involves the use of distance–geometry algorithms. This method, which has been applied with some degree of success to a few small polypeptides,[105,106] is based on the interconvertibility of intramolecular distances, torsion angles and Cartesian coordinates, providing the chirality of the structure is known.[107–110] Although this is possibly the most elegant approach as no initial trial model is required, it suffers from the problem of false minima. The second and third methods both involve starting with an initial trial model which in part reduces the false minimum problem. In the second method, and the one we are currently pursuing, a non-linear least squares optimization procedure is used in which all covalent bond lengths, fixed torsion angles, van der Waals contacts and hydrogen bond lengths and geometries are constrained within narrow limits, in order to refine an initial trial model on the basis of the interproton distance data. In the third method, the initial trial model is refined during the course of a molecular dynamics calculation in which pseudo potentials are used to represent the interproton distance data. Of the two latter approaches, the molecular dynamics method is potentially superior as regards overcoming the false minimum problem but is considerably more expensive in terms of computing time.

The minimum requirement to determine both the glycosidic bond torsion angle (χ) and the sugar pucker conformation, defined in terms of the C4′–C3′ bond torsion angle (δ), is two out of the three intranucleotide sugar–base distances, $r_{H1'-H8/H6}$, $r_{H2'-H8/H6}$, and $r_{H3'-H8/H6}$. The syn and anti ranges for χ are $60 \pm 90°$ and $240 \pm 90°$ respectively. The distance $r_{H1'-H8/H6}$ has a maximum value of 3.7–3.9 Å at $\chi = 240°$ (anti) and a minimum value of 2.3–2.5 Å at $\chi = 60°$ (syn). Furthermore, each value of $r_{H1'-H8/H6}$ is compatible with two values of χ: $60° < \chi_1 < 240°$ and $\chi_2 = (240° - \chi_1) + 240°$. Given the restricted degrees of freedom imposed by the five membered sugar ring, the distance $r_{H2'-H8/H6}$ enables one to distinguish between χ_1 and χ_2 unambiguously and to simultaneously determine the C4′–C3′ bond torsion angle (δ). Similar arguments apply to any other combinations of these three distances. It

goes without saying, of course, that the more distances available, the better the determination of χ and δ, and in this respect the intranucleotide sugar–sugar interproton distances, $r_{H1'-H2'}$, $r_{H2'-H3'}$, and $r_{H2''-H3'}$, are quite helpful, if available.

The C4′–C5′ bond torsion angle (γ) can also be uniquely defined, providing two out of the three intranucleotide distances $r_{H3'-H5''}$, $r_{H4'-H5''}$, and $r_{H4'-H5'}$ are known.

Once the glycosidic bond and sugar pucker conformations are known for each nucleotide, the interresidue interproton distances enable one to define the position of each individual base-pair with respect to its adjacent neighbours either side in terms of approximate values for the P–O5′(α), O5′–C5′(β), C3′–O3′(ε) and O3′–P(ζ) backbone torsion angles, the helical twist, the helical rise and the base tilt. In addition, where at least two distances from the imino proton of one base-pair to protons of the adjacent base-pair (i.e. imino, amino and A(H2) protons) are known, the propellor twist and base roll angles can be defined.

4.4. *Examples*

To date we have determined the solution structures of several oligonucleotides on the basis of the approach outlined in Sections 4.2 and 4.3, principally by manual model building. These include the DNA hexamer 5′d(CGTACG)$_2$ and DNA octamer 5′d(ACGCGCGT)$_2$ which are both characterized by an alternating pyrimidine–purine sequence.[56,57] In the case of both oligonucleotides the overall solution structure is that of right-handed B DNA, namely a right-handed helix with a helical rise of

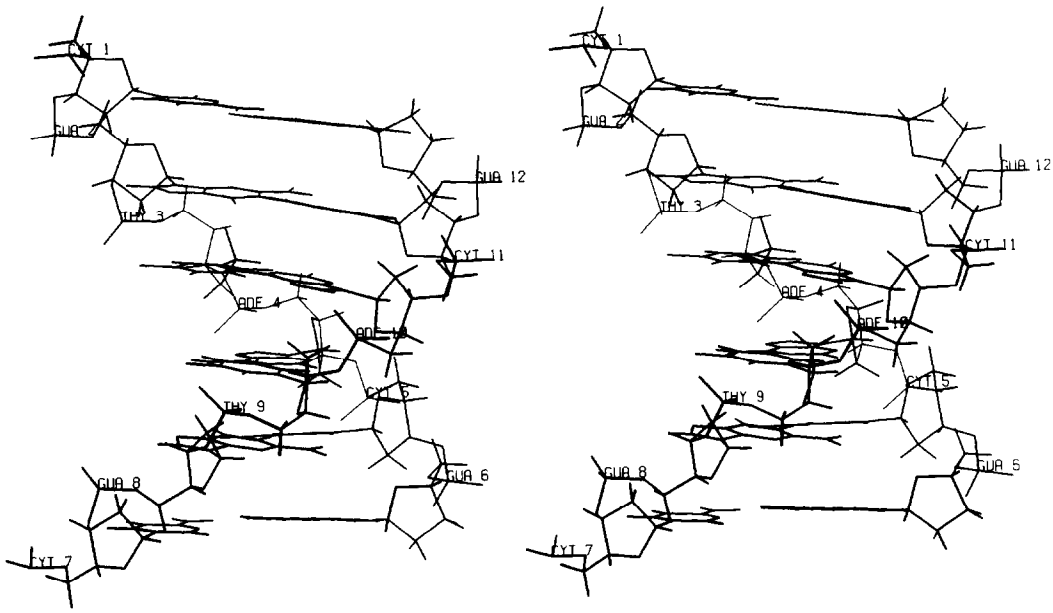

FIG. 23. Stereo view of the refined solution structure of 5′d(CGTACG)$_2$. This structure was generated by a restrained least squares minimization in which all covalent bond lengths, fixed torsion angles, van der Waals contacts, and hydrogen bond lengths and geometry were constrained within narrow limits in order to refine an initial trial model on the basis of 200 interproton distances determined from NOE measurements. The starting coordinates used for the refinement were those of classical B DNA as determined by fibre diffraction.

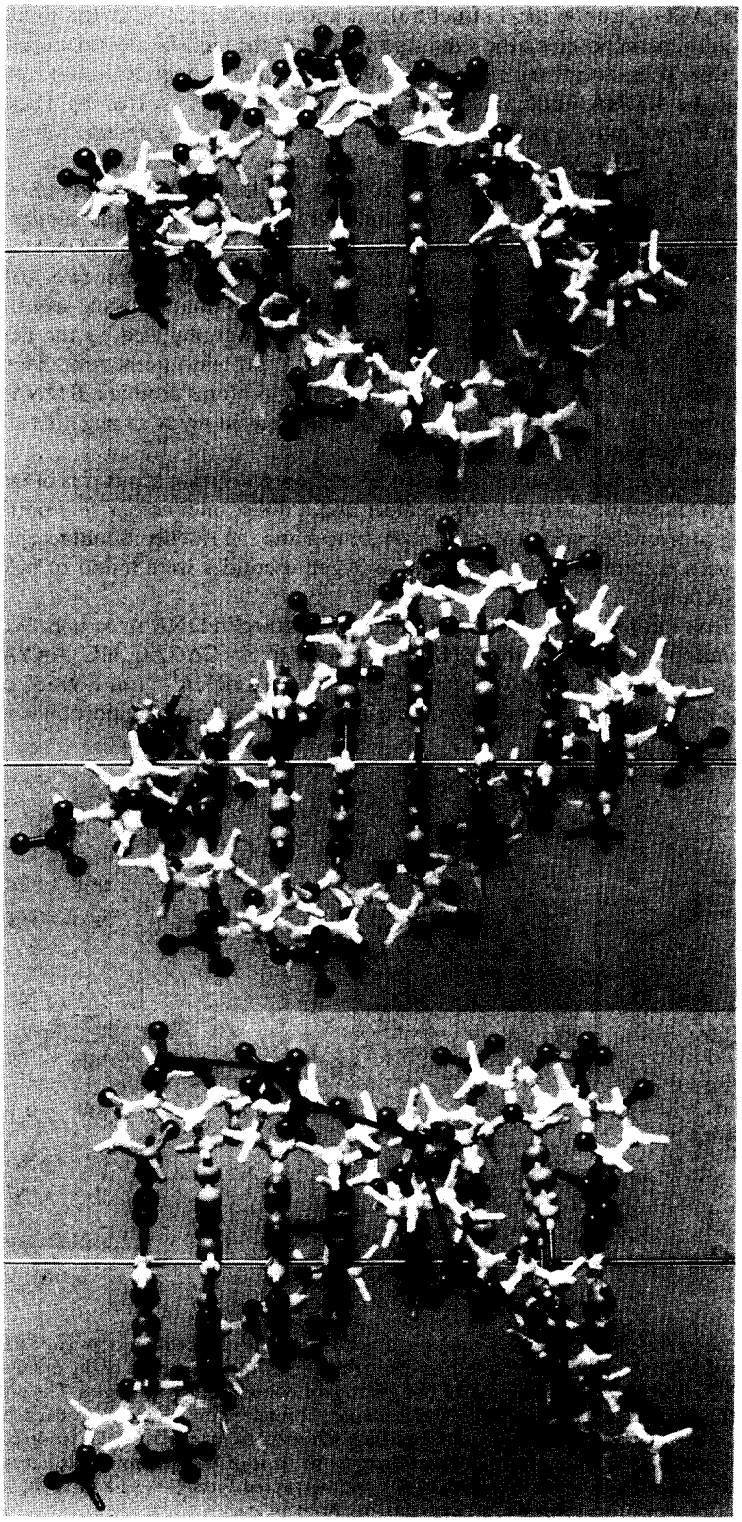

FIG. 24. Three views of the solution structure of 5'd(ACGCGCGT)$_2$, constructed from Nicholson models by manual model building on the basis of interproton distances determined by NOE measurements.[56] The overall structure is that of B DNA. Superimposed on this structure is a dinucleotide repeating unit with alternation in the glycosidic bond, sugar pucker and backbone conformations. The zig-zag appearance of the phosphate backbone is highlighted.

~3.3 Å, ten base-pairs per turn and the base-pairs approximately perpendicular to the helix axis. In the case of 5'd(CGTACG)$_2$, subtle local structural variations associated with the pyrimidine and purine nucleotides are superimposed on the overall structure but the mononucleotide repeating unit is preserved (see Fig. 23). These local structural variations are similar though less marked than in the crystal structure of the B DNA dodecamer 5'd(CGCGAATTCGCG)$_2$ solved by Dickerson and Drew,[6] and this difference may in part be due to weaker intermolecular interactions in solution. In contrast, 5'd(ACGCGCGT)$_2$ has a clear alternating structure with a dinucleotide repeat, alternation occurring in the local helical twist and the glycosidic bond, sugar pucker and phosphodiester backbone conformations (see Fig. 24). This alternating structure is in principle similar to that of wrinkled B DNA found in fibres of poly d(GC)[111] and the model of alternating B DNA proposed by Klug *et al.*[112] However, there are major structural differences between the latter two structures and that of the octamer. The existence of both subtle, and more dramatic, local, sequence-specific variations in the solution structures of DNA oligonucleotides as exemplified by the hexamer and octamer, can clearly have a major influence on specific DNA–protein interactions. Thus, it is not difficult to visualize that the zig-zag distribution of the phosphorus atoms around a B DNA helix, as in the case of the octamer (Fig. 24), can present a specific multifaceted array of negative charges to a potentially interacting protein surface.

In addition to the hexamer and octamer discussed above, low resolution structures of two non self-complementary DNA duplexes, namely an undecamer and a dodecamer comprising portions of the specific DNA target sites for the cyclic AMP receptor protein and the glucocorticoid receptor protein, respectively, have been determined.[58,92] Both these oligonucleotides were found to belong to the right-handed B DNA family.

The strategy we have outlined is not just limited to double-stranded DNA structures. We have also determined the solution structure of the RNA pentadecamer 5'*r* CAGAC$_m$UG$_m$AAYAψm^5CUG comprising the anticodon loop and stem (residues 28 to 42) of yeast tRNA^{Phe} (see Fig. 25), and carried out a comparison of the solution structure with the crystallographic data of that portion of intact yeast

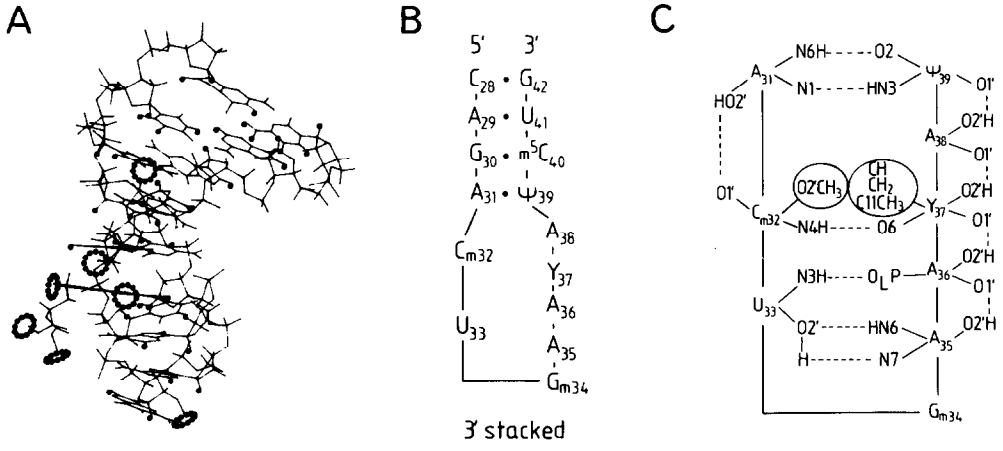

FIG. 25. Diagrammatic representation of the solution structure of the anticodon loop and stem of yeast tRNA^{Phe}.[60] (A) Anticodon loop and stem structure as determined by X-ray diffraction of the monoclinic crystal form of yeast tRNA^{Phe}.[115] Protons have been added using standard bond lengths and angles. The protons whose resonances have been assigned are highlighted. (B) Schematic representation of the 3' stacked hairpin loop structure as found in the crystal and in solution. (C) Stabilizing interactions for the 3' stacked loop conformation of the pentadecamer in solution deduced from model building on the basis of 75 interproton distances determined by NOE measurements. Hydrogen bonds are represented by interrupted lines (----) and groups involved in hydrophobic interactions are encircled.

$tRNA^{Phe}$.[60] The pentadecamer adopts a hairpin loop structure in solution with the loop in a 3′-stacked conformation stabilized by both hydrogen bonding and hydrophobic interactions within the loop. The solution structure is both qualitatively and quantitatively remarkably similar to the crystal structure with an overall root mean square difference of only 1.2 Å between the interproton distances determined by NMR and X-ray crystallography.

Furthermore, single-stranded oligonucleotides which are inherently more flexible than their double-stranded counterparts are amenable to this approach, as has been shown for a single-stranded DNA undecamer.[113] The overall structure of this single-stranded DNA undecamer was found to be that of a right-handed B type helix with extensive base stacking. Within this overall structure there is quite a large degree of variability as exemplified by variations in glycosidic bond and sugar pucker conformation, most likely determined by base sequence.

In the examples given above, we have dealt only with isolated species. The same approach can also be used for interacting systems using transferred nuclear Overhauser enhancement (TRNOE) measurements.[38,39] These simply involve the extension of classical NOE measurements to ex-

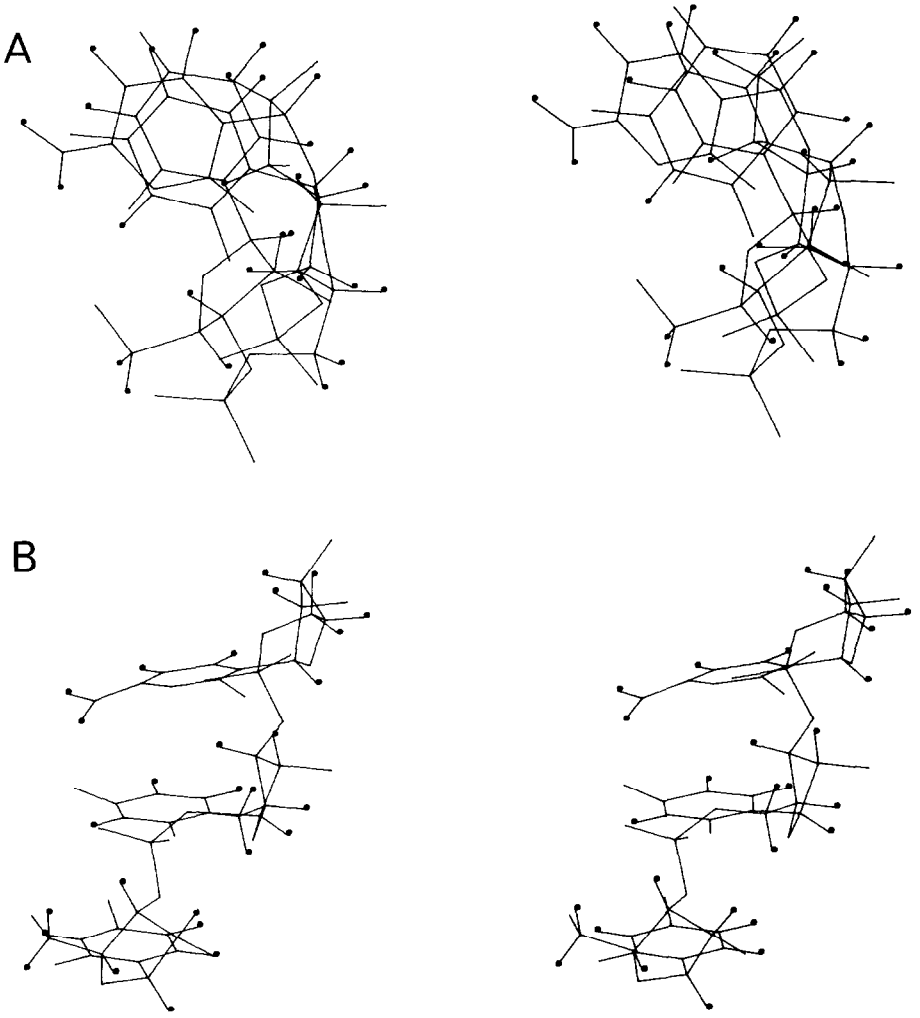

FIG. 26. Two stereoviews of the structure of rUpUpC bound to $tRNA^{Phe}$ deduced from model building on the basis of the interproton distance determined by TRNOE measurements.[47]

changing systems, making use of chemical exchange to transfer magnetization concerning cross-relaxation between bound ligand protons from the bound to the free state. In this manner we have determined the solution structure of the ribotrinucleoside diphosphate rUpUpC, the codon for phenylalanine, bound to yeast $tRNA^{Phe}$.[47] The glycosidic bond and ribose conformations are low anti and 3'-endo, respectively, typical of an A-RNA type structure. The main chain torsion angles are all within the range of those expected for A-RNA but small differences from those of conventional A-RNA 11 result in a special structure (see Fig. 26) with a larger rotation per residue (40 to 45° compared to 32.7° in A-RNA 11) and almost perfect stacking of the bases. These two structural features, which are similar to those found in the anticodon triplet of the monoclinic form of yeast $tRNA^{Phe}$,[114,115] provide the underlying structural basis for the known greater stability of the codon–anticodon complex relative to an equivalent double helical RNA trimer with a conventional A-RNA structure.

5. CONCLUDING REMARKS

In the present review we have outlined the potential of pre-steady state proton–proton NOE measurements to probe the solution structures of small oligonucleotides, the methodology for obtaining interproton distances from the NOE data, and the approaches used to derive solution structures from these interproton distances.

The NOE measurements in solution cannot compete as yet with single crystal X-ray diffraction data in the wealth of structural information they can provide. This is because the NOE data are only capable of providing an interproton distance data set between protons separated by less than 5 Å, whereas high resolution single crystal X-ray diffraction is able to locate the positions of all atoms in space with the exception of protons. The data obtained by the two techniques should be treated as complementary. This is particularly so when the different natures of the solution and crystal structures are borne in mind. Both are average structures with small time dependent fluctuations about a mean as oligonucleotides exhibit some degree of flexibility. However, whereas the crystal structure is a simple linear superposition of all the populations present in the crystal, the distances obtained from NOE measurements in solution are $(\langle r_{ij}^{-6} \rangle)^{-1/6}$ means. Thus, whereas all fluctuations are equally weighted in the crystal structure, the average distance between two protons in the solution structure is weighted in favour of the fluctuations with the shorter interproton distances. In addition, the molecules in the crystal are subject to crystal packing forces. Taking these considerations into account, the interproton distances obtained from NOE measurements should provide a powerful tool supplementing crystallographic studies, particularly in cases where crystal data are not available, in comparative studies of oligonucleotides with an array of different sequences, and in the study of transitions between different conformational states of DNA.

Moreover, using TRNOE measurements[38,39] it will be possible to probe the conformations of oligonucleotides bound to large macromolecules such as proteins and tRNA, an area which should prove particularly fruitful as crystallization of such complexes has been extremely difficult and in many cases not possible.

Acknowledgements—This work was supported by the Medical Research Council (GMC and AMG) and the Lister Institute of Preventive Medicine (GMC). All NMR spectra were recorded on the AM500 spectrometer of the Medical Research Council Biomedical NMR Centre at the National Institute for Medical Research.

REFERENCES

1. J. D. WATSON and F. H. C. CRICK, *Nature* **171**, 737 (1953).
2. M. H. F. WILKINS, E. R. STOKES and H. R. WILSON, *Nature* **171**, 738 (1953).
3. R. E. FRANKLIN and R. G. GOSLING, *Nature* **171**, 740 (1953).
4. G. H. GASSEN and A. LANG, *Chemical and Enzymatic Synthesis of Gene Fragments—A Laboratory Manual*, Verlag Chemie, Mannheim (1982).
5. R. M. WING, H. R. DREW, T. TAKANO, C. BROKA, S. TANAKA, K. ITAKURA and R. E. DICKERSON, *Proc. Natl. Acad. Sci. U.S.A.* **78**, 2179 (1981).
6. R. E. DICKERSON and H. R. DREW, *J. Mol. Biol.* **149**, 751 (1981).

7. H. R. DREW and R. E. DICKERSON, *J. Mol. Biol.* **151**, 535 (1981).
8. Z. SHAKKED, D. RABINOVICH, W. B. T. CRUSE, E. EGERT, O. KENNARD, G. SALA, S. A. SALISBURY and M. A. VISWAMITRA, *Proc. R. Soc. Lond. Ser. B.* **213**, 479 (1981).
9. Z. SHAKKED, D. RABINOVICH, O. KENNARD, W. B. T. CRUSE, S. A. SALISBURY and A. VISWAMITRA, *J. Mol. Biol.* **166**, 183 (1983).
10. B. N. CONNER, T. TAKANO, S. TANAKA, K. ITAKURA and R. E. DICKERSON, *Nature* **295**, 294 (1982).
11. B. N. CONNER, C. YOON, J. L. DICKERSON and R. E. DICKERSON, *J. Mol. Biol.* **174**, 663 (1984).
12. A. H. J. WANG, G. J. QUIGLEY, F. J. KOLPAK, J. L. CRAWFORD, J. H. VAN BOOM, G. VAN DER MAREL and A. RICH, *Nature* **282**, 680 (1979).
13. A. H. J. WANG, G. J. QUIGLEY, F. J. KOLPAK, G. VAN DER MAREL, J. H. VAN BOOM and A. RICH, *Science* **211**, 171 (1981).
14. H. R. DREW, T. TAKANO, S. TANAKA, K. ITAKURA and R. E. DICKERSON, *Nature* **286**, 567 (1980).
15. H. R. DREW and R. E. DICKERSON, *J. Mol. Biol.* **152**, 723 (1981).
16. S. ARNOTT, R. CHANDRASEKARAN, D. L. BIRSALL, A. G. W. LESLIE and R. L. RATCLIFF, *Nature* **283**, 743 (1980).
17. S. ARNOTT and R. CHANDRASEKARAN, In: *Biomolecular Stereodynamics* (Ed. R. H. SARMA) p. 199, Adenine Press, New York (1981).
18. S. ARNOTT, R. CHANDRASEKARAN, I. H. HALL, L. C. PUIGJAUER, J. K. WALKER and M. WANG, *Cold Spring Harbor Symp. Quant. Biol.* **47**, 53 (1983).
19. D. RHODES, In: *Topics in Nucleic Acid Structures, Part 2*, Ed. S. NEIDLE, p. 287, MacMillan Press, London (1982).
20. R. H. SARMA, B. G. WARNER and C. K. MITRA, In: *Biomolecular Stereodynamics* (Ed. R. H. SARMA) Vol. 1, p. 89, Adenine Press, New York (1982).
21. D. J. PATEL, S. A. KOZLOWSKI and S. BHATT, *Proc. Natl. Acad. Sci. U.S.A.* **80**, 3908 (1983).
22. L. S. KAN, D. M. CHENG, K. JAYARAMAN, E. E. LEUTZINGER, P. S. MILLER and P. O. P. TS'O, *Biochemistry* **21**, 6723 (1982).
23. R. A. BELL, D. ALKEMA, J. M. CADDINGTON, P. A. HADER, D. W. HUGHES and T. NEILSON, *Nucl. Acids Res.* **11**, 1143 (1983).
24. O. JARDETZKY and G. C. K. ROBERTS, *NMR in Molecular Biology*, Academic Press, New York (1981).
25. J. R. MELLEMA, C. A. G. HAASNOOT, J. H. VAN BOOM and C. ALTONA, *Biochem. Biophys. Acta* **655**, 256 (1981).
26. S. TRAN-DINH, J. M. NEWMAN, T. HUYUH-DINH, B. GEMISSEL, J. IGOLEN and G. SIMONOT, *Eur. J. Biochem.* **124**, 415 (1982).
27. C. ALTONA RECUIL, *J. R. Netherlands Chem. Soc.* **101**, 413–433.
28. M. Karplus, *J. Am. Chem. Soc.* **85**, 2870 (1963).
29. J. H. NOGGLE and R. E. SCHIRMER, *The Nuclear Overhauser Effect—Chemical Applications*, Academic Press, New York (1971).
30. J. K. M. SANDERS and J. D. MERSCH, *Prog. Nucl. Magn. Reson. Spectrosc.* **15**, 291 (1982).
31. F. M. POULSEN, J. C. HOSCH and C. J. DOBSON, *Biochemistry* **19**, 2956 (1980).
32. G. WAGNER, A. KUMAR and K. WÜTHRICH, *Eur. J. Biochem.* **114**, 375 (1981).
33. G. WAGNER and K. WÜTHRICH, *J. Mol. Biol.* **159**, 347 (1982).
34. G. WAGNER and K. WÜTHRICH, *J. Mol. Biol.* **160**, 334 (1982).
35. S. A. ARSENIEV, G. WIDER, F. J. JOUBERT and K. WÜTHRICH, *J. Mol. Biol.* **159**, 323 (1982).
36. P. ŠTROP, G. WIDER and K. WÜTHRICH, *J. Mol. Biol.* **166**, 641 (1983).
37. M. P. WILLIAMSON, D. MARION and K. WÜTHRICH, *J. Mol. Biol.* **173**, 341 (1984).
38. G. M. CLORE and A. M. GRONENBORN, *J. Magn. Reson.* **48**, 402 (1982).
39. G. M. CLORE and A. M. GRONENBORN, *J. Magn. Reson.* **53**, 423 (1983).
40. G. M. CLORE and A. M. GRONENBORN, *FEBS Lett.* **145**, 197 (1982).
41. G. M. CLORE, A. M. GRONENBORN, S. E. MITCHINSON and N. M. GREEN, *Eur. J. Biochem.* **128**, 113 (1982).
42. A. M. GRONENBORN and G. M. CLORE, *J. Mol. Biol.* **157**, 155 (1982).
43. A. M. GRONENBORN and G. M. CLORE, *Biochemistry* **21**, 4040 (1982).
44. A. M. GRONENBORN, G. M. CLORE and J. JEFFERY, *J. Mol. Biol.* **172**, 559 (1982).
45. A. M. GRONENBORN, G. M. CLORE, M. BRUNORI, B. GIARDINA, G. FALCIONI and M. F. PERUTZ, *J. Mol. Biol.* **178**, 731 (1984).
46. J. P. ALBRAND, B. BIRDSALL, J. FEENEY, G. C. K. ROBERTS and A. S. V. BURGEN, *Int. J. Biolog. Macromol.* **1**, 37 (1979).
47. G. M. CLORE, A. M. GRONENBORN and L. W. MCLAUGHLIN, *J. Mol. Biol.* **174**, 163 (1984).
48. P. D. JOHNSTON and A. G. REDFIELD, *Nucl. Acids Res.* **5**, 3913 (1978).
49. S. ROY and A. G. REDFIELD, *Biochemistry* **22**, 1386 (1983).
50. D. R. HARE and B. R. REID, *Biochemistry* **21**, 5129 (1982).
51. A. HEERSCHAP, C. A. G. HAASNOOT and C. W. HILBERS, *Nucl. Acids Res.* **10**, 6981 (1982).
52. A. HEERSCHAP, C. A. G. HAASNOOT and C. W. HILBERS, *Nucl. Acids Res.* **11**, 4483 (1983).
53. A. HEERSCHAP, C. A. G. HAASNOOT and C. W. HILBERS, *Nucl. Acids Res.* **11**, 4501 (1983).
54. D. G. REID, S. A. SALISBURY, S. BELLARD, Z. SHAKKED and D. H. WILLIAMS, *Biochemistry* **22**, 2012 (1983).
55. D. G. REID, S. A. SALISBURY, T. BROWN, D. H. WILLIAMS, J. J. VASSEUR, B. RAYNER and J. L. IMBACH, *Eur. J. Biochem.* **135**, 307 (1983).
56. G. M. CLORE and A. M. GRONENBORN, *EMBO J.* **2**, 2109 (1983).

57. A. M. GRONENBORN, G. M. CLORE and B. J. KIMBER, *Biochem. J.* **221**, 723 (1984).
58. G. M. CLORE and A. M. GRONENBORN, *Eur. J. Biochem.* **141**, 119 (1984).
59. A. M. GRONENBORN, G. M. CLORE, M. B. JONES and J. JIRICNY, *FEBS Lett.* **165**, 216 (1984).
60. G. M. CLORE, A. M. GRONENBORN, E. A. PIPER, L. W. MCLAUGHLIN, E. GRAESER and J. H. VAN BOOM, *Biochem. J.* **221**, 737 (1984).
61. R. M. SCHEEK, N. RUSSO, R. BOELENS, R. KAPTEIN and J. H. VAN BOOM, *J. Am. Chem. Soc.* **105**, 2914 (1983).
62. R. M. SCHEEK, R. BOELENS, N. RUSSO, J. H. VAN BOOM and R. KAPTEIN, *Biochemistry* **23**, 1371 (1984).
63. D. R. HARE, D. E. WEMMER, S. H. CHOU, G. DROBNY and B. R. REID, *J. Mol. Biol.* **171**, 319 (1983).
64. M. A. WEISS, D. J. PATEL, R. T. SAUER and M. KARPLUS, *Proc. Natl. Acad. Sci. U.S.A.* **81**, 130 (1984).
65. J. FEIGON, J. M. WRIGHT, W. LEUPIN, W. A. DENNY and D. R. KEARNS, *J. Am. Chem. Soc.* **104**, 5540 (1982).
66. J. FEIGON, W. LEUPIN, W. A. DENNY and D. R. KEARNS, *Biochemistry* **22**, 5943 (1983).
67. D. FRECHET, D. M. CHENG, L. S. KAN and P. O. P. TS'O, *Biochemistry* **22**, 5194 (1983).
68. I. SOLOMON, *Phys. Rev.* **90**, 559 (1955).
69. A. KALK and H. C. J. BERENDSEN, *J. Magn. Reson.* **24**, 743 (1976).
70. G. WAGNER and K. WÜTHRICH, *J. Magn. Reson.* **33**, 675 (1979).
71. C. M. DOBSON, E. T. OLEJNICZAK, F. M. POULSEN and R. G. RATCLIFFE, *J. Magn. Reson.* **48**, 97 (1982).
72. A. KUMAR, G. WAGNER, R. R. ERNST and K. WÜTHRICH, *J. Am. Chem. Soc.* **103**, 3654 (1981).
73. S. MACURA and R. R. ERNST, *Mol. Phys.* **41**, 95 (1980).
74. J. JEENER, B. H. MEIER, P. BACHMAN and R. R. ERNST, *J. Chem. Phys.* **71**, 4546 (1979).
75. S. MACURA, Y. HUANG, D. SUTER and R. R. ERNST, *J. Magn. Reson.* **43**, 259 (1981).
76. G. WIDER, S. MACURA, A. KUMAR, R. R. ERNST and K. WÜTHRICH, *J. Magn. Reson.* **56**, 207 (1984).
77. R. BAUMANN, G. WIDER, R. R. ERNST and K. WÜTHRICH, *J. Magn. Reson.* **44**, 402–406.
78. A. J. STATES, R. A. HABERKORN and D. J. RUBEN, *J. Magn. Reson.* **48**, 286 (1982).
79. D. MARION and K. WÜTHRICH, *Biochem. Biophys. Res. Commun.* **113**, 967 (1983).
80. S. ALEXANDER, *Rev. Sci. Instrum.* **32**, 1066 (1961).
81. A. G. REDFIELD, S. D. KUNZ and E. K. RALPH, *J. Magn. Reson.* **19**, 114 (1975).
82. A. G. REDFIELD and S. D. KUNZ, In: *NMR and Biochemistry*, Eds. S. J. OPELLA and P. LU, p. 225, Dekker, New York (1981).
83. J. M. WRIGHT, J. FEIGON, W. DENNY, W. LEUPIN and D. R. KEARNS, *J. Magn. Reson.* **45**, 514 (1981).
84. P. PLATEAU and M. GUERON, *J. Am. Chem. Soc.* **104**, 7310 (1982).
85. G. M. CLORE, B. J. KIMBER and A. M. GRONENBORN, *J. Magn. Reson.* **54**, 170 (1983).
86. V. SKLENÁŘ and Z. STARĚNK, *J. Magn. Reson.* **50**, 495 (1982).
87. P. J. HOURE, *J. Magn. Reson.* **55**, 283 (1983).
88. K. ROTH, B. J. KIMBER and J. FEENEY, *J. Magn. Reson.* **41**, 302 (1980).
89. C. A. G. HAASNOOT and C. W. HILBERS, *Biopolymers* **22**, 1259 (1983).
90. D. M. CHENG and R. W. SARMA, *J. Am. Chem. Soc.* **99**, 7333 (1977).
91. G. M. CLORE and A. M. GRONENBORN, *FEBS Lett.* **172**, 219 (1984).
92. G. M. CLORE, H. LAUBLE, T. FRENKIEL and A. M. GRONENBORN, *Eur. J. Biochem.* **145** (1984) in press.
93. M. E. HOGAN and O. JARDETZKY, *Proc. Natl. Acad. Sci. U.S.A.* **76**, 6341 (1979).
94. M. E. HOGAN and O. JARDETZKY, *Biochemistry* **19**, 3460 (1980).
95. R. L. RILL, P. R. HILLIARS, L. F. LEVY and G. C. LEVY, In: *Biomolecular Stereodynamics*, Ed. R. H. SARMA, Vol. 1, p. 383, Adenine Press, New York (1982).
96. H. SHINDO, *Biopolymers* **19**, 509 (1980).
97. G. LIPARI and A. SZABO, *Biochemistry* **20**, 6250 (1981).
98. P. H. BOLTON and T. L. JAMES, *J. Am. Chem. Soc.* **102**, 25 (1980).
99. P. H. BOLTON and T. L. JAMES, *Biochemistry* **19**, 1388 (1980).
100. S. R. HOLBROOK and S. H. KIM, *J. Mol. Biol.* **173**, 361 (1984).
101. P. KOLLMAN, J. W. KEEPERS and P. WEINER, *Biopolymers* **21**, 2345 (1982).
102. M. LEVITT, *Cold Spring Harbor Symp. Quant. Biol.* **47**, 251 (1983).
103. B. TIDOR, K. K. IRIKURA, B. R. BROOKS and M. KARPLUS, *J. Biol. Struct. Dyn.* **1**, 231 (1983).
104. G. M. CLORE and A. M. GRONENBORN, *FEBS Lett.* **175**, 117 (1984).
105. W. BRAUN, G. WIDER, K. H. LEE and K. WÜTHRICH, *J. Mol. Biol.* **109**, 921 (1983).
106. S. A. ARSENIEV, V. I. KONDAKOV, V. N. MAIOROV and V. F. BYSTROV, *FEBS Lett.* **165**, 57 (1984).
107. G. M. CRIPPEN and T. F. HAVEL, *Acta Crystallogr.* **A34**, 282 (1978).
108. F. E. COHEN and M. J. E. STERNBERG, *J. Mol. Biol.* **138**, 321 (1980).
109. W. BRAUN, C. BOSCH, C. R. BROWN, N. GO and K. WÜTHRICH, *Biochim. Biophys. Acta.* **667**, 377 (1981).
110. K. WÜTHRICH, G. WIDER, G. WAGNER and W. BRAUN, *J. Mol. Biol.* **155**, 311 (1982).
111. S. ARNOTT, R. CHANDRASEKARAN, L. C. PUIGJANER, J. K. WALKER, J. H. HALL, D. L. BIRSALL and R. L. RATCLIFFE, *Nucl. Acids Res.* **11**, 1457 (1983).
112. A. KLUG, A. JACK, M. A. VISWAMITRA, O. KENNARD, Z. SHAKKED and T. A. STEITZ, *J. Mol. Biol.* **131**, 669 (1979).
113. G. M. CLORE and A. M. GRONENBORN, *Eur. Biophys. J.* **11**, 95 (1984).
114. A. JACK, J. E. HARDING and A. KLUG, *J. Mol. Biol.* **108**, 619 (1976).
115. B. HINGERTY, R. S. BROWN and A. JACK, *J. Mol. Biol.* **124**, 523 (1978).
116. J. W. KEEPERS and T. L. JAMES, *J. Magn. Reson.* **57**, 404 (1984).